Organometallics **2000,** *19,* 3032−3053

1,3-Dipolar Cycloaddition to the Fe−X=C Fragment 18. Chemoselectivity in the Addition of Activated Alkynes across the Fe−O=C Fragment vs the Fe−N=C Fragment in Chelate (α-Imino ester)tricarbonyliron Complexes

Ron Siebenlist, Mireille de Beurs, Nantko Feiken, Hans-Werner Frühauf,*,† and Kees Vrieze

Inorganic Laboratory, Institute of Molecular Chemistry, University of Amsterdam, Nieuwe Achtergracht 166, 1018 WV Amsterdam, The Netherlands

Huub Kooijman, Nora Veldman, Miles T. Lakin, and Anthony L. Spek*

Bijvoet Center for Biomolecular Research, Crystal and Structural Chemistry, Utrecht University, Padualaan 8, 3584 CH Utrecht, The Netherlands

Received December 22, 1999

In situ prepared chelate complexes $Fe(CO)_3(R^1N{=}C(R^2)C(R^3){=}O)$ (R^1 = alkyl, R^2 = H, R^3 = O-alkyl) (**7a**−**j**) react with dimethyl acetylenedicarboxylate (DMAD) via a 1,3-dipolar cycloaddition reaction to form four products as a result of cycloaddition to both the Fe−O=C and the Fe−N=C fragments. The main product is the $Fe(CO)_3$(butenolide) complex (**10**), which results from cycloaddition to the Fe−O=C fragment, indicating that this fragment is more reactive than the Fe−N=C fragment. Complexes **10**, **11**, **13**, and **15** have been characterized by spectroscopy (IR, ^{1}H and ^{13}C NMR, FD-mass) and by elemental analyses. The molecular structures of all four types of complexes (**10d**, **11a**, **13c**, and **15h**) have been established by single-crystal X-ray diffraction. The product formation and distribution is determined by both the R^1 and the R^3 substituents. Reaction with the less activated alkyne methyl propynoate (MP) results, in a slow reaction, exclusively in cycloaddition to the Fe−O=C fragment with formation of two products depending on the additional ligand offered. Uptake of an additional CO ligand leads to the $Fe(CO)_3$(butenolide) complex **16**, which is formed exclusively as one of the possible regioisomers with the former ketone carbon atom C−C connected to the ester-substituted alkyne carbon atom. When MP also acts as an additional ligand, the tricyclic complexes **20** are formed, which consist of three five-membered rings. Complexes **20** are also obtained in almost quantitative yield by irradiation of **16** in the presence of MP. Similarly, complexes **19** are obtained by irradiation of **10** in the presence of MP. The molecular structure has been confirmed by an X-ray structure determination of **19c**. When complexes **10** are refluxed in THF and subsequently reacted with water at room temperature, the organic butenolide derivatives **21** with an exocyclic enamine function are obtained. The molecular structure has been established by an X-ray structure determination of **21c**. Reaction of **10** under 50 bar of CO pressure at 115 °C results in the liberation of the intact butenolide heterocycles (**22**) together with some side products.

Introduction

In previous parts of this series we reported on the reactions of $M(CO)_2L(R^1\text{-DAB})$ (M = Fe, Ru; L = CO, CNR) complexes (**1**) with dimethyl acetylenedicarboxylate (DMAD)[1] and methyl propynoate (MP),[1] which have been shown to give synthetically interesting coordinated heterocycles, e.g., 1,5-dihydropyrrol-2-one (**4**) and 1,4,3a,6a-tetrahydropyrrolo[3,2-*b*]pyrrole (THPP;[1] **5**) (cf. Scheme 1: X = NR^1, R^3 = H).[2−7]

The initial step in these reactions represents an oxidative 1,3-dipolar cycloaddition of the dipolarophile, e.g. an activated alkyne, across the M−N=C fragment (the 1,3-dipole), resulting in the formation of the bicyclo[2.2.1] intermediate **2**. The subsequent reaction of intermediate **2** (X = NR^1) and, accordingly, the product

---

[†] E-mail: hwf@anorg.chem.uva.nl. Fax: +31-20-525 6456.

(1) The abbreviations used most frequently throughout this text are as follows: R-DAB: 1,4-diaza-1,3-butadienes of formula $R^1N{=}C(H)C(H){=}NR^1$; THPP, 1,4,3a,6a-tetrahydropyrrolo[3,2-*b*]pyrrole; DMAD, dimethyl acetylenedicarboxylate; MP, methyl propynoate; *t*-Am, 2-methyl-2-butyl. The other acronyms are explained at the appropriate places in the text.

(2) de Lange, P. P. M.; Frühauf, H.-W.; van Wijnkoop, M.; Kraakman, M. J. A.; Kranenburg, M.; Groot, A. H. J. P.; Fraanje, J.; Wang, Y.; Numan, M. *Organometallics* **1993**, *12*, 417.

(3) Frühauf, H.-W.; Seils, F.; Goddard, R. J.; Romão, M. J. *Angew. Chem., Int. Ed. Engl.* **1983**, *22*, 992; *Angew. Chem.* **1983**, *95*, 1014; *Angew. Chem., Suppl.* **1983**, 1435.

(4) Frühauf, H.-W.; Seils, F.; Goddard, R. J.; Romão, M. J. *Organometallics* **1985**, *4*, 948.

(5) Frühauf, H.-W.; Seils, F. *J. Organomet. Chem.* **1986**, *302*, 59.

(6) Frühauf, H.-W.; Seils, F. *J. Organomet. Chem.* **1987**, *323*, 67.

(7) van Wijnkoop, M.; de Lange, P. P. M.; Frühauf, H.-W.; Vrieze, K.; Wang, Y.; Goubitz, K.; Stam, C. H. *Organometallics* **1992**, *11*, 3607.

10.1021/om991027y CCC: $19.00
Publication on Web 07/06/2000

Scheme 1. Reactions of $Fe(CO)_2L$(R-DAB), $Fe(CO)_3$(α-imino ketone), and $Ru(CO)_3$(R-DAB) with the Electron-Deficient Alkynes DMAD and MP

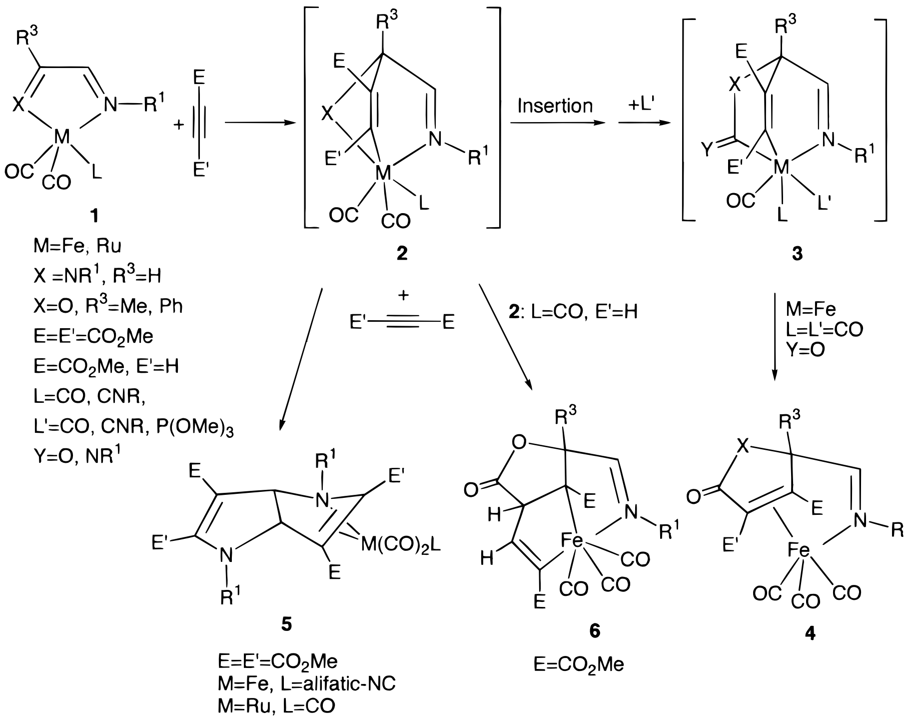

formation depend on the coligand L, the additional ligand L′, the metal M, and the substitution pattern of both R-DAB and the activated alkyne. First, **2** can intramolecularly react further by insertion of CO or CNR (R = aryl), followed by the uptake of an additional ligand L′, resulting in the stable bicyclo[2.2.2] complex **3**. Second, **2** can react intermolecularly with a second molecule of DMAD to give the doubly cycloadded product $M(CO)_2$(L)(THPP) (**5**). Iron complex **3** may, in the case of L = L′ = CO, undergo reductive elimination, resulting, after recoordination of the double bond, in the formation of the $Fe(CO)_3$(pyrrolinone) complexes **4**.

To expand the synthetic potential of the organometal 1,3-dipolar cycloaddition reaction, we also investigated the reactions of the closely related σ(N):σ(O)-coordinated $Fe(CO)_3$(α-imino ketone) complexes (**1**: X = O, R^3 = Me, Ph) toward DMAD[8] and MP[9] and found that they exhibit similar reactivity. The exclusive formation of the $Fe(CO)_3$(butenolide) complexes **4** indicates that in the latter reactions the initial 1,3-dipolar cycloaddition of the activated alkyne proceeds with complete chemoselectivity across the $\mathrm{Fe{-}O{=}C}$ fragment. This indicates that the $\mathrm{Fe{-}O{=}C}$ fragment is more reactive than the $\mathrm{Fe{-}N{=}C}$ fragment due to both electronic and steric reasons. The enhanced reactivity of the $\mathrm{Fe{-}O{=}C}$ fragment is further corroborated by the reaction conditions with the less activated dipolarophile MP. The $\mathrm{Fe{-}O{=}C}$ fragment in $Fe(CO)_3$(α-imino ketone) readily reacts with MP at −30 °C, while for complete reaction with MP of the $\mathrm{Fe{-}N{=}C}$ fragment in $Fe(CO)_3$(*i*-Pr-DAB)[10] several days of refluxing in ether is necessary. Furthermore, the reaction with MP resulted in the new $Fe(CO)_3$-(tricyclic) complex **6**, in which a second molecule of MP has been incorporated.[9]

These results prompted us to investigate the 1,3-dipolar reactivity of mononuclear chelate complexes of α-imino esters, i.e., the σ(N):σ(O) chelate $Fe(CO)_3(R^1N{=}C(R^2)C(R^3){=}O)$ (R^1 = alkyl, R^2 = H, R^3 = O-alkyl). As has been stated previously,[2,7−10] the $\mathrm{Fe{-}X{=}C}$ fragment can be characterized as a nucleophilic or type I dipole,[11−15] according to the Sustmann classification. In cycloaddition reactions of this type of 1,3-dipoles, the interaction between the dipole HOMO and the dipolarophile LUMO is predominant. Consequently, as has been shown by Houk et al.,[16−18] the introduction of an electron-withdrawing group on a terminal of this type of 1,3-dipole will lower the reactivity. In the present case, the ester alkoxy group should thus lower the 1,3-dipolar reactivity of the $\mathrm{Fe{-}O{=}C}$ fragment and could lead to competition between cycloaddition over the $\mathrm{Fe{-}O{=}C}$ and $\mathrm{Fe{-}N{=}C}$ fragments.

In this article we report on the 1,3-dipolar cycloaddition reactions of $Fe(CO)_3$(α-imino ester) complexes (**7**) with the electron-deficient alkynes DMAD and MP. Complexes **7** are in situ prepared by reaction of $R^1N{=}C(H)C(R^3){=}O$ with $Fe_2(CO)_9$. Reaction of **7** with DMAD

---

(8) van Wijnkoop, M.; Siebenlist, R.; de Lange, P. P. M.; Frühauf, H.-W.; Vrieze, K.; Smeets, W. J. J.; Spek, A. L. *Organometallics* **1993**, *12*, 4172.

(9) van Wijnkoop, M.; Siebenlist, R.; Ernsting, J. M.; de Lange, P. P. M.; Frühauf, H.-W.; Horn, E.; Spek, A. L. *J. Organomet. Chem.* **1993**, *482*, 99 and references therein.

(10) de Lange, P. P. M.; de Boer, R. P.; van Wijnkoop, M.; Ernsting, J. M.; Frühauf, H.-W.; Vrieze, K.; Smeets, W. J. J.; Spek, A. L. *Organometallics* **1993**, *12*, 440.

(11) Sustman, R. *Tetrahedron Lett.* **1971**, 2721.

(12) Sustman, R.; Trill, H. *Angew. Chem., Int. Ed. Engl.* **1972**, *11*, 838.

(13) Sustman, R. *Pure. Appl. Chem.* **1974**, *40*, 569.

(14) Herndon, W. C. *Chem. Rev.* **1972**, *72*, 157.

(15) Houk, K. N.; Yamaguchi, K. In *1,3-Dipolar Cycloaddition Chemistry*; Padwa, A., Ed.; Wiley: New York, 1984; Chapter 13, p 407.

(16) Houk, K. N. *Acc. Chem. Res.* **1975**, *8*, 361.

(17) Houk, K. N.; Sims, J.; Duke, R. E.; Strozier, R. W.; George, J. K. *J. Am. Chem. Soc.* **1973**, *95*, 7287.

(18) Houk, K. N.; Sims, J.; Watts, C. R.; Luskus, L. J. *J. Am. Chem. Soc.* **1973**, *95*, 7301.

Table 1. Syntheses of Complexes 10, 11,[a] 13, and 15

	ligand substituent					yield (%)		
ligand	R^1	R^3	amt of ligand (mmol)[b]	amt of $\mathrm{Fe_2(CO)_9}$ (g (mmol))	amt of DMAD (μL)	**10**	**13**	**15**
a	*n*-Pr	OMe	7.74	4.64 (9.29)	1046	12	6	
b	*neo*-Pe	OMe	6.36	2.78 (7.63)	860	17		~1[c]
c	*i*-Pr	OMe	7.74	4.64 (9.29)	1046	30	9	~1[c]
d	*i*-Pr	OEt	6.98	3.05 (8.38)	944	26		~1[c]
e	*i*-Pr	O*i*-Pr	6.36	2.78 (7.63)	860	16		~2[c]
f	*t*-Bu	OMe	6.98	3.05 (8.38)	944	64		4
g	*t*-Bu	OEt	6.36	2.78 (7.63)	860	61		5
h	*t*-Bu	O*i*-Pr	5.48	2.39 (6.58)	741	30		10
i	*t*-Am	OMe	6.36	2.78 (7.63)	860	59		4[c]
j	*t*-Am	OEt	5.48	2.39 (6.58)	741	58		4[c]

[a] Complexes **11** are formed in ca. 1% yield, based on NMR (see Experimental Section). [b] Based on 1.0 g of α-imino ketone. [c] Yields based on NMR (see Experimental Section).

Table 2. Syntheses of Complexes 16 and 20

	ligand substituents				yield (%)			
ligand	R^1	R^2	amt of ligand (mmol)[a]	amt of $\mathrm{Fe_2(CO)_9}$ (g (mmol))	**16**[b]	**20**[b]	**16**[c]	**20**[c]
c	*i*-Pr	OMe	3.87	1.69 (4.64)		2		3
f	*t*-Bu	OMe	3.49	1.52 (4.19)	21	2	8	7
i	*t*-Am	OMe	3.18	1.39 (3.82)	24	2	6	8%

[a] Based on 0.5 g of the respective α-imino ketone. [b] Yields when 1 equiv of MP is added dropwise. [c] Yields when 2 equiv of MP is added in one lot.

leads to the formation of four products as a result of cycloaddition over both the Fe−O=C and Fe−N=C fragments. Reaction with MP leads to a regioselective cycloaddition over exclusively the Fe−O=C fragment, resulting in two products. The X-ray molecular structures of the formed organometallic complexes are described. Finally, some decomplexation reactions of the organic moiety of **10** are studied.

Experimental Section

Materials and Apparatus. ^{1}H and ^{13}C NMR spectra were recorded on a Bruker AMX-300 spectrometer. The IR spectra were recorded on Perkin-Elmer 283 and Biorad FTIR-7 spectrophotometers. Elemental analyses were carried out by Dornis & Kolbe, Microanalytisches Laboratorium, Mülheim a. d. Ruhr, Germany. Solvents were carefully dried and distilled under nitrogen prior to use. All preparations were carried out under an atmosphere of dry nitrogen by conventional Schlenk techniques. The irradiations were carried out using a Philips HPK 125 W high-pressure mercury lamp. Silica gel for column chromatography (Kieselgel 60, 70−230 mesh, E. Merck, Darmstadt, Germany) was dried and activated prior to use by heating to 180 °C under vacuum for 16 h. $\mathrm{Fe(CO)_5}$ (Strem Chemicals) and dimethyl, diethyl, and diisopropyl L-tartrates (Aldrich) were used as commercially obtained. $\mathrm{Fe_2(CO)_9}$[19] and the α-imino esters **b**−**h** have been prepared by published procedures.[20]

The new α-imino esters $\mathrm{R^1N{=}C(H)C(OMe){=}O}$ with R^1 = *n*-propyl (**a**) and $\mathrm{R^1N{=}C(H)C(OEt){=}O}$ with R^1 = 2-methyl-2-butyl (*t*-Am)[1] (**j**) were prepared by reaction of respectively methyl or ethyl glyoxylate[21] with the corresponding amines according to published procedures.[20] Yield: **a**, 20%; **j**, 65%. IR (ν; pentane, cm^{-1}): **a**, 1761 m, 1735 s $\nu(\mathrm{CO_2Me})$, 1653 w $\nu(\mathrm{C{=}N})$; **j**, 1761 m, 1728 s $\nu(\mathrm{CO_2Me})$, 1653 w $\nu(\mathrm{C{=}N})$. ^{1}H NMR ($\mathrm{CDCl_3}$, room temperature, δ in ppm relative to TMS): **a**, 7.63 (1H, t, 1.2 Hz, $\mathrm{N{=}C}H$), 3.79 (s, 3H, $\mathrm{OC}H_3$), 3.52 (2H, dt, 1.2 Hz, 7.0 Hz, $\mathrm{NC}H_2$), 1.60 (2H, dt, 7.0 Hz, 7.4 Hz, $\mathrm{NCH_2C}H_2$), 0.77 (3H, t, 7.4 Hz, $\mathrm{NCCC}H_3$); **j**, 7.60 (1H, s, $\mathrm{N{=}C}H$), 4.35 (2H, q, 7.1 Hz, $\mathrm{OC}H_2$), 1.64 (2H, q, 7.5 Hz, $\mathrm{C}H_2\mathrm{CH_3}$), 1.35 (3H, t, 7.1 Hz, $\mathrm{OCH_2C}H_3$), 1.21 (6H, s, $\mathrm{C(C}H_3)_2$), 0.78 (3H, t, 7.5 Hz, $\mathrm{CH_2C}H_3$). ^{13}C NMR ($\mathrm{CDCl_3}$, room temperature, δ in ppm relative to TMS): **a**, 162.8 (C=O), 149.2 (C=N), 67.4 (NCH$_2$), 50.9 (OCH$_3$), 22.4 (NCH$_2C$H$_2$), 11.4 (CH$_2C$H$_3$); **j**, 162,4 (C=O), 148.2 (C=N), 60.6 (NC), 60.2 (OCH$_2$), 34.2 (C(CH$_3$)$_2$), 25.1 (CCH$_2$), 13.2 (OCH$_2C$H$_3$), 7.5 (CH$_2C$H$_3$).

General procedures for the preparations are given below; details are listed in Tables 1 and 2.

Synthesis of 10a−j, 11a,f, 13a,c, and 15f−h by Reaction of $\mathrm{Fe(CO)_3(R^1N{=}C(H)C(R^3){=}O)}$ (7a−j) with DMAD. The in situ cycloaddition reaction of $\mathrm{Fe(CO)_3(}$*n*-$\mathrm{PrN{=}C(H)C(OMe){=}O)}$ (**7a**) is described as a representative example. A 1.0 g (7.74 mmol) portion of the α-imino ester **a** was added to a stirred suspension of 3.38 g (9.29 mmol, 1.2 equiv) of $\mathrm{Fe_2(CO)_9}$ in 40 mL of THF at room temperature, whereupon the solution turned deep purple, indicating the formation of **7a**. Immediately a solution of 1046 μL (8.5 mmol, 1.1 equiv) of DMAD in 20 mL of THF was added dropwise at such a rate that all **7a** just reacted (ca. 1 drop/3 s); i.e., the solution became pale yellow. During the reaction the solution became dark brown and, when all the $\mathrm{Fe_2(CO)_9}$ and ligand had reacted, the reaction mixture was stirred for another 15 min. After evaporation of the solvent, the remaining dark brown oily residue was redissolved in 5 mL of $\mathrm{CH_2Cl_2}$ and the products were separated by column chromatography on silica gel. The reactions with ligands **b**−**j** were performed analogously (for details see Table 1). The product separation by column chromatography is described for all reactions. Elution with pentane/$\mathrm{Et_2O}$ (9:1) afforded in all cases a brown-orange fraction containing traces of $\mathrm{Fe_2(CO)_6}$(α-imino ester).

Subsequent elution with pentane/$\mathrm{Et_2O}$ (2:3) afforded for ligands **a** and **c** an orange-brown fraction that was evaporated to dryness. The resulting orange-brown powder was washed twice with 10 mL of pentane/$\mathrm{Et_2O}$ (9:1) and dried in vacuo, yielding **13a**,**c** as bright orange powders in 6% (**13a**) and 9% (**13c**) yields. To obtain deep orange crystals of **13a**,**c**, $\mathrm{CH_2Cl_2}$ was slowly added to a suspension of **13a**,**c** in $\mathrm{Et_2O}$ until the

---

(19) $\mathrm{Fe_2(CO)_9}$ was prepared by a slightly modified literature procedure using a quartz Schlenk tube and starting with 25 mL of $\mathrm{Fe(CO)_5}$, 150 mL of glacial acetic acid, and 10 mL of acetic anhydride (the last was added to prevent the mixture containing too much water). A Rayonet RS photochemical reactor ($\lambda_{\max}$ = 2500 Å) was used for irradiation, and a continuous stream of air was used to cool the reaction mixture. Filtering, washing with water, ethanol, and ether, and subsequent drying in vacuo gave $\mathrm{Fe_2(CO)_9}$ in usually more than 90% yield: Braye, E. H.; Hübel, W. *Inorg. Synth.* **1966**, *8*, 178.

(20) van der Poel, H.; van Koten, G. *Synth. Commun.* **1978**, *8*, 305.

(21) Kelly, R. T.; Schimdt, T. E.; Haggerty, J. G. *Synthesis* **1972**, 544.

product was completely dissolved, followed by cooling to −60 °C for several days. Crystals of **13c** were suitable for X-ray diffraction. For the other ligands, **b** and **d**−**j**, no identifiable complexes were eluted with pentane/Et_2O (2:3). In all cases, elution with Et_2O/CH_2Cl_2 (9:1) afforded a yellow-brown fraction that was evaporated to dryness. The brownish yellow residue was washed three times with 20 mL of pentane/Et_2O (3:1) (the washings were collected) and dried in vacuo, yielding $Fe(CO)_3$(butenolide) (**10a**−**j**) as yellow powders in 12−64% yield depending on the α-imino ester used. Crystalline material was obtained by slow addition of CH_2Cl_2 to suspensions of **10a**−**j** in Et_2O until the product was completely dissolved, followed by cooling to −60 °C for 2 days. Crystals of **10c** were suitable for X-ray diffraction.

The collected pentane/Et_2O washings (see above) were evaporated to dryness, resulting in a dark brown oily residue. The ^1H NMR spectra revealed the presence of complexes **11a**−**j** and **15b**−**e,** respectively (cf. Table 1), together with small amounts of **10a**−**j**. The remaining dark brown residue was suspended in 10 mL of pentane, and Et_2O was added until a clear brown-black solution was obtained. For ligands **f**−**h**, crystallization at −60 °C gave pale yellow crystals of $Fe(CO)_4$(pyrrolinone) (**15f**−**h**) in 4, 5, and 10% yields, respectively. Analytically pure samples were obtained by recrystallization from pentane/Et_2O (5:1), resulting in off-white crystals. Crystals of **15g** were suitable for X-ray diffraction. For ligand **a**, black crystals of $Fe_2(CO)_5$[OIB(*n*-Pr,H,OMe)][22] (**11a**) were obtained upon cooling to −60 °C in ca. 1% yield together with crystalline **10a**. Crystals of **11a** were suitable for X-ray diffraction. From the mother liquor of **15f**, dissolved in pentane, black crystals of **11f** were obtained (ca. 1%) together with **10f** and **15f**. Because complexes **11** were obtained in very low yield in combination with crystals of other complexes, no elemental analyses were done. The ^1H and ^{13}C NMR data of **11a**,**f** were obtained from these mixtures.

Synthesis of 16c,f,i by Reaction of $Fe(CO)_3(R^1N{=}C(H)C(OMe){=}O)$ (7c,f,i) with MP. Method a. The in situ cycloaddition reaction of $Fe(CO)_3$(*i*-PrN═C(H)C(OMe)═O) (**7c**) is described as a typical example. A 0.5 g (3.87 mmol) portion of the α-imino ester **c** was added to a stirred suspension of 1.69 g (4.64 mmol, 1.2 equiv) of $Fe_2(CO)_9$ in 40 mL of THF at room temperature, whereupon the solution turned deep purple, indicating the formation of **7c**. Immediately a solution of 380 μL (4.2 mmol, 1.1 equiv) of MP in 20 mL of THF was added dropwise at the same rate as for the reactions with DMAD. During the reaction the solution became dark brown, and when all the $Fe_2(CO)_9$ and ligand had reacted, the reaction mixture was stirred for another 15 min. After evaporation of the solvent, the remaining dark brown oily residue was redissolved in 5 mL of CH_2Cl_2 and the products were separated by column chromatography on silica gel. The reactions with ligands **f** and **i** were performed and chromatographed analogously (cf. Table 2 for details).

Elution with pentane/Et_2O (9:1) afforded in all cases a brown-orange fraction containing traces of $Fe_2(CO)_6$(α-imino ester). Subsequent elution with pentane/Et_2O (2:3) afforded a deep yellow fraction that was evaporated to dryness. The yellow residue was washed twice with 10 mL of pentane/Et_2O (3:1), yielding $Fe(CO)_3$(butenolide) (**16f**,**i**) as bright yellow powders in 21% and 24% yields, respectively. Yellow crystals were obtained by crystallization from Et_2O/CH_2Cl_2 (9:1) at −60 °C. For ligand **c** no identifiable complexes were obtained with this eluent. Subsequent elution with Et_2O/CH_2Cl_2 (4:1) afforded a pale yellow fraction that was evaporated to dryness. The yellow oily residue was dissolved in 2 mL of Et_2O, and slowly 15 mL of pentane was added, the resulting precipitate was washed twice with 10 mL of pentane dried in vacuo, yielding $Fe(CO)_3$(tricyclus) (**20c**,**f**,**i**) as pale yellow powders in 2% yield.

Method b. A 0.5 g (3.87 mmol) portion of the α-imino ester **c** and 700 μL (7.8 mmol, 2 equiv) of MP was added in one lot to a stirred suspension of 1.55 g (4.64 mmol, 1.2 equiv) of $Fe_2(CO)_9$ in 40 mL of THF at room temperature. During the reaction the solution became dark brown and, when all the $Fe_2(CO)_9$ and ligand had reacted, the reaction mixture was stirred for another 15 min. After evaporation of the solvent, the remaining dark brown oily residue was redissolved in 5 mL of CH_2Cl_2 and the products were purified by column chromatography on silica gel as mentioned for method a. The reactions with ligands **f** and **i** were performed analogously (cf. Table 2 for details).

Photochemical Preparation of Complexes 19c,f,i from 10c,f,i. The synthesis of **19c** is described as a typical example. In a Pyrex glass immersion well apparatus, a solution of 300 mg (0.62 mmol) of **10c** and 160 μL (1.8 mmol; 3 equiv) of MP in 40 mL of THF was irradiated at room temperature with a high-pressure mercury lamp. The reaction was followed by IR spectroscopy. Complete conversion of the starting complex took approximately 5 h, during which time the color of the solution changed from yellow to brown. The dark brown oily residue obtained after evaporation of the solvent was redissolved in 3 mL of CH_2Cl_2, and **19c** was purified by column chromatography. Complexes **19f**,**i** were prepared and chromatographed analogously. Elution with Et_2O/CH_2Cl_2 (4:1) afforded a yellow fraction that was evaporated to dryness. The yellow oily residue was dissolved in 2 mL of Et_2O, and then slowly 15 mL of pentane was added. The resulting precipitate was washed twice with 10 mL of pentane and dried in vacuo, yielding $Fe(CO)_3$(tricyclic) (**19c**,**f**,**i**) as pale yellow powders in 27, 37, and 38% yields, respectively. Pale yellow crystals were obtained by slow addition of CH_2Cl_2 to suspensions of **19c**,**f**,**i** in Et_2O until the product was completely dissolved, followed by cooling to −60 °C for 2 days. Crystals of **19c** were suitable for X-ray diffraction.

Photochemical Preparation of Complexes 20c,f,i from 16c,f,i. Complexes **20** were prepared by a procedure analogous to that described for **19c** (see above). The yields were 85−90%.

Synthesis of 21c,f,i. The synthesis of **21c** is described as a typical example. A solution of 500 mg (1.03 mmol) of **10c** in 60 mL of THF was stirred at 70 °C. The reaction was monitored by IR spectroscopy and was stopped when the CO stretching bands of **9c** had disappeared (approximately 2 h), during which time the color of the reaction mixture changed from yellow to a transparent dark brown. The reaction mixture was cooled to room temperature and 180 μL (10 mmol) of H_2O was added, whereupon the solution turned intense yellow-brown. Subsequently the reaction mixture was evaporated to dryness and **21c** was purified by column chromatography. Compounds **21f**,**i** were prepared and chromatographed analogously. Elution with CH_2Cl_2 afforded a yellow fraction containing impurities. Consecutive elution with CH_2Cl_2/THF (1:1) afforded an intensely yellow fraction that was evaporated to dryness, giving **21** in ca. 70% yield as yellow sticky powders. Crystalline samples were obtained by slow addition of CH_2Cl_2 to a suspension of **20** in Et_2O until the product was completely dissolved, followed by cooling to −60 °C for several days. Crystals of **21c** were suitable for X-ray diffraction.

Decomplexation of the Butenolide Ligand 22 from 10c−j. The decomplexation of **10c** is described as a typical example. A solution of 500 mg (1.03 mmol) of **10c** in 200 mL of toluene was placed in an autoclave under 50 bar of CO and heated to 115 °C. The reaction was monitored by IR spectroscopy and was stopped when the CO stretching bands of **10c** had disappeared (approximately 30−60 min). The reaction mixture was immediately removed from the autoclave, cooled to room temperature, and evaporated to dryness, resulting in a brown tar. The brown tar was twice extracted with 50 mL

---

[22] OIB(R^1,R^2,R^3) is the abbreviation for the organic ligand resulting from C−C bond formation between $R^1N{=}C(R^2)C(R^3){=}O$ and the alkyne EC≡CE (E = CO_2Me). The backbone of the ligand is $R^1N{=}C(R^2)C(R^3)(O)C(E){=}CE$, which is 4-imino-1-buten-3-olato.

Table 3. Crystal Data and Details of the Structure Determination of 10c, 11a, 13c, 15h, 19c, and 21c

	10d	**11a**	**13c**	**15h**	**19c**	**21c**
			Crystal Data			
empirical formula	$C_{17}H_{19}FeNO_{10}$	$C_{17}H_{17}Fe_2NO_{11}$	$C_{18}H_{17}Fe_2NO_{12}$	$C_{20}H_{23}FeNO_{11}$	$C_{20}H_{21}FeNO_{12}$	$C_{12}H_{15}NO_6$
fw	453.19	523.02	551.03	509.25	523.13	269.25
cryst syst	monoclinic	monoclinic	triclinic	monoclinic	monoclinic	orthorhombic
space group	$P2_1/c$ (No. 14)	$C2/c$ (No. 15)	$P\bar{1}$ (No. 2)	$P2_1/c$ (No. 14)	$P2_1/c$ (No. 14)	$Pbca$ (No. 61)
a (Å)	15.3007(16)	30.666(4)	10.260(3)	9.8445(8)	13.6361(6)	11.5210(11)
b (Å)	12.533(3)	9.2337(9)	10.4843(14)	17.972(2)	9.4202(6)	12.0740(10)
c (Å)	11.024(3)	14.8832(15)	11.0383(14)	14.3774(14)	17.4590(9)	19.4168(11)
α (deg)	90	90	89.726(11)	90	90	90
β (deg)	106.987(15)	103.617(9)	87.15(2)	114.933(8)	96.392(5)	90
γ (deg)	90	90	75.67(2)	90	90	90
V (Å^3)	2021.8(8)	4095.9(8)	1149.0(4)	2306.7(4)	2228.8(2)	2701.0(4)
Z	4	8	2	4	4	8
D_{calcd} (g/cm^3)	1.489	1.696	1.593	1.466	1.559	1.324
F(000) (e)	936	2128	560	1056	1080	1136
μ (cm^{-1})	7.9 (Mo Kα)	14.7 (Mo Kα)	107.3 (Cu Kα)	7.1 (Mo Kα)	7.4 (Mo Kα)	8.7 (Cu Kα)
cryst size (mm)	0.4 × 0.5 × 0.8	0.02 × 0.15 × 0.15	0.3 × 0.3 × 0.4	0.2 × 0.23 × 0.25	0.4 × 0.4 × 0.4	0.2 × 0.4 × 0.4
			Data Collection			
temp (K)	298	150	295	150	150	295
θ_{min}, θ_{max} (deg)	1.4, 27.5	1.4, 27.5	4.0, 75.0	1.9, 27.5	1.2, 27.5	2.3, 75.0
SET4 θ_{min}, θ_{max} (deg)	11.29, 15.76 (25 rflns)	8.25, 15.00 (25 rflns)	13.31, 26.33 (25 rflns)	10.10, 14.01 (25 rflns)	11.51, 13.89 (25 rflns)	16.37, 24.82 (25 rflns)
wavelength (Å)	0.710 73 (Mo Kα)	0.710 73 (Mo Kα)	1.541 84 (Cu Kα)	0.710 73 (Mo Kα)	0.710 73 (Mo Kα)	1.541 84 (Cu Kα)
filter/mon	Zr filter	graphite mon	Ni filter	graphite mon	graphite mon	Ni filter
$\Delta\omega$ (deg)	0.71 + 0.35 tan θ	0.83 + 0.35 tan θ	0.68 + 0.14 tan θ	0.72 + 0.35 tan θ	0.66 + 0.35 tan θ	0.68 + 0.14 tan θ
horiz, vert aperture (mm)	3.00, 4.00	2.75, 4.00	2.52. 6.00	3.00, 4.00	3.00, 4.00	3.00. 6.00
X-ray exposure time (h)	78	93	71	16	38	33
linear instab (%)	4	3	1	2	2	<1
ref rflns	$60\bar{6}$, $\bar{4}\bar{2}1$, $21\bar{4}$	$20\bar{8}$, $\bar{6}\bar{2}3$, $\bar{8}02$	$\bar{2}1\bar{3}$, $\bar{2}2\bar{3}$, $\bar{3}\bar{2}\bar{2}$	$2\bar{3}\bar{2}$, 123, $23\bar{2}$	$\bar{2}\bar{3}\bar{3}$, $\bar{3}\bar{2}\bar{4}$, $\bar{4}1\bar{2}$	$\bar{2}\bar{2}3$, $\bar{3}\bar{2}\bar{1}$, $\bar{1}\bar{5}2$
data set	−19 to +19, 0−16, −14 to +14	−39 to +38, −11 to 0, −17 to +19	−12 to +12, −13 to +13, −13 to +12	−8 to +12, −23 to 0, −18 to +16	−12 to +9, −17 to +17, −22 to +22	−14 to 0, −15 to 0, 0−24
total no. of data	5775	9316	8468	6020	16235	4287
total no. of unique data	4629	4674	4725	5294	5116	2776
R_{int}	0.044	0.086	0.087	0.063	0.046	0.007
no. of obsd data	3058 ($I > 2.5\sigma(I)$)	no crit applied	no crit applied	no crit applied	no crit applied	no crit applied
abs cor range		0.92−1.08 (DIFABS)	0.60−1.85 (DIFABS)			
			Refinement			
no. of refined params	264	284	303	305	313	180
final R1[a]	0.0521 (3058, $I > 2.5\sigma(I)$)	0.0609 (2481, $I > 2\sigma(I)$)	0.0829 (3112, $I > 2\sigma(I)$)	0.0760 (2623, $I > 2\sigma(I)$)	0.0351 (4071, $I > 2\sigma(I)$)	0.0470 (2210, $I > 2\sigma(I)$)
final wR2[b]		0.0976	0.2403	0.1392	0.0828	0.1416
final R_w[c]	0.0740					
goodness of fit	1.370	0.902	1.063	0.943	1.044	1.054
w^{-1} [d]	$\sigma^2(F) + 0.00063P^2$	$\sigma^2(F^2) + (0.0255P)^2$	$\sigma^2(F^2) + (0.1381P)^2$	$\sigma^2(F^2) + (0.0414P)^2$	$\sigma^2(F^2) + (0.0360P)^2 + 0.76P$	$\sigma^2(F^2) + (0.0866P)^2 + 0.41P$
$(\Delta/\sigma)_{av}$, $(\Delta/\sigma)_{max}$	0.014, 0.061	0.000, 0.003	0.001, 0.025	0.000, 0.002	0.001, 0.036	0.001, 0.003
min, max resd dens (e/Å^3)	−0.47, 0.51	−0.49, 0.58	−1.38, 1.40 (near Fe)	−0.45, 0.44	−0.32, 0.36	−0.23, 0.26

[a] $R1 = \sum||F_o| - |F_c||/\sum|F_o|$. [b] $wR2 = [\sum[w(F_o^2 - F_c^2)^2]/\sum[w(F_o^2)^2]]^{1/2}$. [c] $R_w = [\sum[w(||F_o| - |F_c||)^2]/\sum[w(F_o^2)]]^{1/2}$. [d] $P = (\mathrm{Max}(F_o^2, 0) + 2F_c^2)/3$.

of pentane, giving a pale yellow solution that after evaporation of the solvent yielded a yellow oil in ca. 80% yield. The reactions with **10d**−**j** were performed analogously. The butenolides **22f**,**g**,**i**,**j** were isolated in ca. 90−95% purity. Attempted purification by column chromatography resulted in (partial) decomposition. Butenolide **22h** was formed in approximately 30% yield together with several side products. The ^{1}H and ^{13}C NMR data were derived from this mixture. Decomplexation of the butenolide ligands in **10c**−**e** resulted, besides the desired free butenolides **22c**−**e**, in two other products. The ^{1}H and ^{13}C NMR data for the butenolides **22c**,**d** were derived from the mixture. One of the newly formed products could be isolated from the mixture because the butenolide and the other new product decomposed upon attempted separation on silica gel. Elution with THF gave pale yellow fractions containing **23c**−**e** in 15, 20, and 35% yields, respectively. Crystallization from Et_2O gave off-white crystalline material. When they are stirred at room temperature, the free butenolides (**22**) do not isomerize to the corresponding compounds **23**. All free butenolides are unstable even when stored at −30 °C and decompose within a few weeks to several unidentified products.

Crystal Structure Determinations of 10d, 11a, 13c, 15h, 19c, and 21c. Crystals suitable for X-ray diffraction were glued to the tip of a glass fiber and transferred into the cold nitrogen stream on an Enraf-Nonius CAD4-T diffractometer on a rotating anode (**11a**, **15h**, and **19c**) or to an Enraf-Nonius CAD4-F diffractometer in a sealed tube at room temperature (**10d**, **13c**, and **21c**). Accurate unit-cell parameters and an orientation matrix were determined by least-squares fitting of the setting angles of a set of well-centered reflections (SET4).[23] The unit-cell parameters were checked for the presence of higher lattice symmetry.[24] Crystal data and details on data collection and refinement are collected in Table 3. All data were collected in the $\omega/2\theta$ scan mode.

---

(23) Boer, J. L.; Duisenberg, A. J. M. *Acta Crystallogr.* **1984**, *A40*, 410.

(24) Spek, A. L. *J. Appl. Crystallogr.* **1988**, *21*, 578.

Table 4. Combinations of Substituents of α-Imino Ester Ligands $R^1N{=}C(H)C(R^3){=}O$ (a−j)

	a	b	c	d	e	f	g	h	i	j
R^1	*n*-Pr	*neo*-Pe	*i*-Pr	*i*-Pr	*i*-Pr	*t*-Bu	*t*-Bu	*t*-Bu	*t*-Am	*t*-Am
R^3	OMe	OMe	OMe	OEt	O-*i*-Pr	OMe	OEt	O-*i*-Pr	OMe	OEt

Data were corrected for *Lp* effects and for the observed linear decay of the reference reflections. For compound **10d** the standard deviations of the intensities as obtained by counting statistics were increased according to an analysis of the excess variance of the reference reflections: $\sigma^2(I) = \sigma_{CS}{}^2(I) + (0.03I)^2$.[25] An empirical absorption correction was applied for compounds **11a** and **13c** (DIFABS);[26] no absorption correction was applied for the other compounds.

The structure of **21c** was solved by automated direct methods (SHELXS86).[27] The structures of the other compounds were solved by automated Patterson methods and subsequent difference Fourier techniques (DIRDIF-92[28] for **10d**, **13c**, and **19c** and SHELXS86[27] for **11a** and **15h**).

Compound **10d** was refined on *F* by full-matrix least-squares techniques (SHELX76).[29] All other structures were refined on F^2 using full-matrix least-squares techniques (SHELXL-93);[30] no observance criterion was applied during refinement on F^2. Hydrogen atoms were included in the refinement on calculated positions, riding on their carrier atoms, except for the amine hydrogen of **21c**, which was located on a difference Fourier map and subsequently included in the refinement.

All methyl hydrogen atoms were refined in a rigid group, allowing for rotation around the C−C and C−O bonds. The non-hydrogen atoms of all structures were refined with anisotropic displacement parameters. Hydrogen atoms of **10d** were refined with one overall isotropic displacement parameter amounting to 0.127(6) Å^2. The hydrogen atoms of the other compound are refined with a fixed isotropic displacement parameter related to the value of the equivalent isotropic displacement parameter of their carrier atoms by a factor of 1.5 for the methyl and freely refined amine hydrogen atoms and 1.2 for the other hydrogen atoms.

Compound **10d** was refined using neutral scattering factors taken from Cromer and Mann,[31] amplified with anomalous dispersion corrections from Cromer and Liberman.[32] For the other compounds, neutral atom scattering factors and anomalous dispersion corrections were taken from ref 33. Geometrical calculations and illustrations were performed with PLATON;[34] all calculations were performed on a DEC station 5000 cluster.

Results and Discussion

The employed ligands and complexes discussed in this section are given in Table 4 and Schemes 2−4, respectively. The α-imino ester ligands are differentiated by the letters **a**−**j**. The type of complex is identified by Arabic numbers.

Reaction of $Fe_2(CO)_9$ with Ligands a−j. Reaction of the α-imino esters $R^1N{=}C(H)C(R^3){=}O$ (**a**−**j**) with $Fe_2(CO)_9$ in THF at room temperature results in the initial formation of the intensely purple or blue chelate $Fe(CO)_3(R^1N{=}C(H){-}C(R^3){=}O)$[35] complexes (**7a**−**j**), according to eq 1.

$$Fe_2(CO)_9 + \mathbf{a{-}j} \rightarrow \underset{\mathbf{7a{-}j}}{Fe(CO)_3(R^1N{=}C(H){-}C(R^3){=}O)} + 2CO + Fe(CO)_5 \quad (1)$$

Unfortunately, however, the mononuclear complexes **7a**−**j** are unstable under the reaction conditions and they react readily to form several mononuclear and binuclear complexes. Therefore, the 1,3-dipolar cycloaddition reactions of **7a**−**j** have to be performed in situ, i.e., adding the dipolarophile, DMAD or MP, to a stirred suspension of $Fe_2(CO)_9$ and the respective α-imino ester.

Reaction of $Fe(CO)_3$(α-iminoester) (7a−j) with DMAD. In situ prepared $Fe(CO)_3$(α-imino ester) (**6a**−**j**) reacts readily at room temperature with DMAD to give a total of four complexes as a result of cycloaddition over both the Fe−O═C and Fe−N═C fragments. The product distribution and formation depends on the R^1 and the R^3 substituent.

Cycloaddition over the Fe−O═C fragment results in the formation of two products (cf. Scheme 2a). The main product is the $Fe(CO)_3$(butenolide) complex (**10**), which is formed in moderate to good yield depending on the ligand used. The additional CO ligand needed for the formation of **10** is produced during the formation of the starting complexes **7** (cf. eq 1). Complexes **10a**−**j** have been characterized by spectroscopy (IR, ^1H NMR, ^{13}C NMR) and elemental analyses. The molecular structure has been confirmed by a single-crystal X-ray diffraction analysis of complex **10d**. The other product, $Fe_2(CO)_5[R^1N{=}C(H)C(R^3)(O)C(CO_2Me){=}C(CO_2Me)]$ (**11a**−**j**; abbreviated as $Fe_2(CO)_5$(OIB),[22] is a binuclear complex which is formed in very low yield for all ligands employed. Complexes **11a**,**f** have been characterized by spectroscopy and by X-ray crystallography (**11a**).

Cycloaddition over the Fe−N═C fragment also results in the formation of two products. The product distribution depends on the bulkiness of the R^1 substituent. The binuclear complexes $Fe_2(CO)_6[R^1N(H)C(CO_2Me)C(CO_2Me)C(CO_2Me)]$ (**13a**, R^1 = *n*-Pr; **13c**, R^1 = *i*-Pr) are formed via reaction of the initial cycloadduct **12** with iron carbonyl before CO insertion into the Fe−N bond has taken place. In complexes **13** the former imine proton has undergone a 1,2-H shift to nitrogen. The $Fe(CO)_4$(pyrrolinone) complexes (**15b**−**j**) are formed when insertion of CO into the Fe−N bond in **12** is faster than the reaction with iron carbonyl. The observed reaction sequence is similar to that observed for $Fe(CO)_3$(R-DAB) (cf. Scheme 1; X = NR^1, R^3 = H). In the present case, this results in the formation of intermediate **14**. Subsequent substitution of the weakly coordinated carboxyl oxygen in **14** by CO gives the final product **15**. The molecular structures are confirmed by single-crystal X-ray determinations of **13c** and **15h**.

Reaction with Methyl Propynoate. In situ prepared $Fe(CO)_3$(α-imino ester) (**7c**,**f**,**i**) reacts slowly at

---

(25) McCandisch, L. E.; Stout, G. H. *Acta Crystallogr.* **1975**, *A31*, 245.

(26) Walker, N.; Stuart, D. *Acta Crystallogr., Sect. A* **1983**, *A39*, 158.

(27) Sheldrick, G. M. SHELXS86, Program for Crystal Structure Determination; University of Göttingen, Göttingen, Germany, 1986.

(28) Beurskens, P. T.; Admiraal, G.; Beurskens, G.; Bosman, W. P.; García-Granda, S.; Gould, R. O.; Smits, J. M. M.; Smykalla, C. The DIRDIF Program System; Technical report of the Crystallography Laboratory; University of Nijmegen, Nijmegen, The Netherlands, 1992.

(29) Sheldrick, G. M. SHELX76, Crystal Structure Analysis Package; University of Cambridge, Cambridge, England, 1976.

(30) Sheldrick, G. M. SHELXL-93, Program for Crystal Structure Determination; University of Göttingen: Göttingen, Germany, 1993.

(31) Cromer, D. T.; Mann, J. B. *Acta Crystallogr., Sect. A* **1968**, *A24*, 321.

(32) Cromer, D. T.; Liberman, D. *J. Chem. Phys.* **1970**, *53*, 1891.

(33) Wilson, A. J. C. *International Tables for Crystallography*; Kluwer Academic: Dordrecht, The Netherlands, 1992.

(34) Spek, A. L. *Acta Crystallogr., Sect. A* **1990**, *A46*, C34.

(35) Siebenlist, R.; Frühauf, H.-W.; Vrieze, K.; Kooijman, H.; Spek, A. L. *Organometallics* **2000**, 19, 3016−3031.

Scheme 2. Cycloaddition of DMAD to (a, top) the Fe–O=C Fragment and (b, bottom) the Fe–N=C Fragment of Fe(CO)$_3$(α-imino ester) (7)

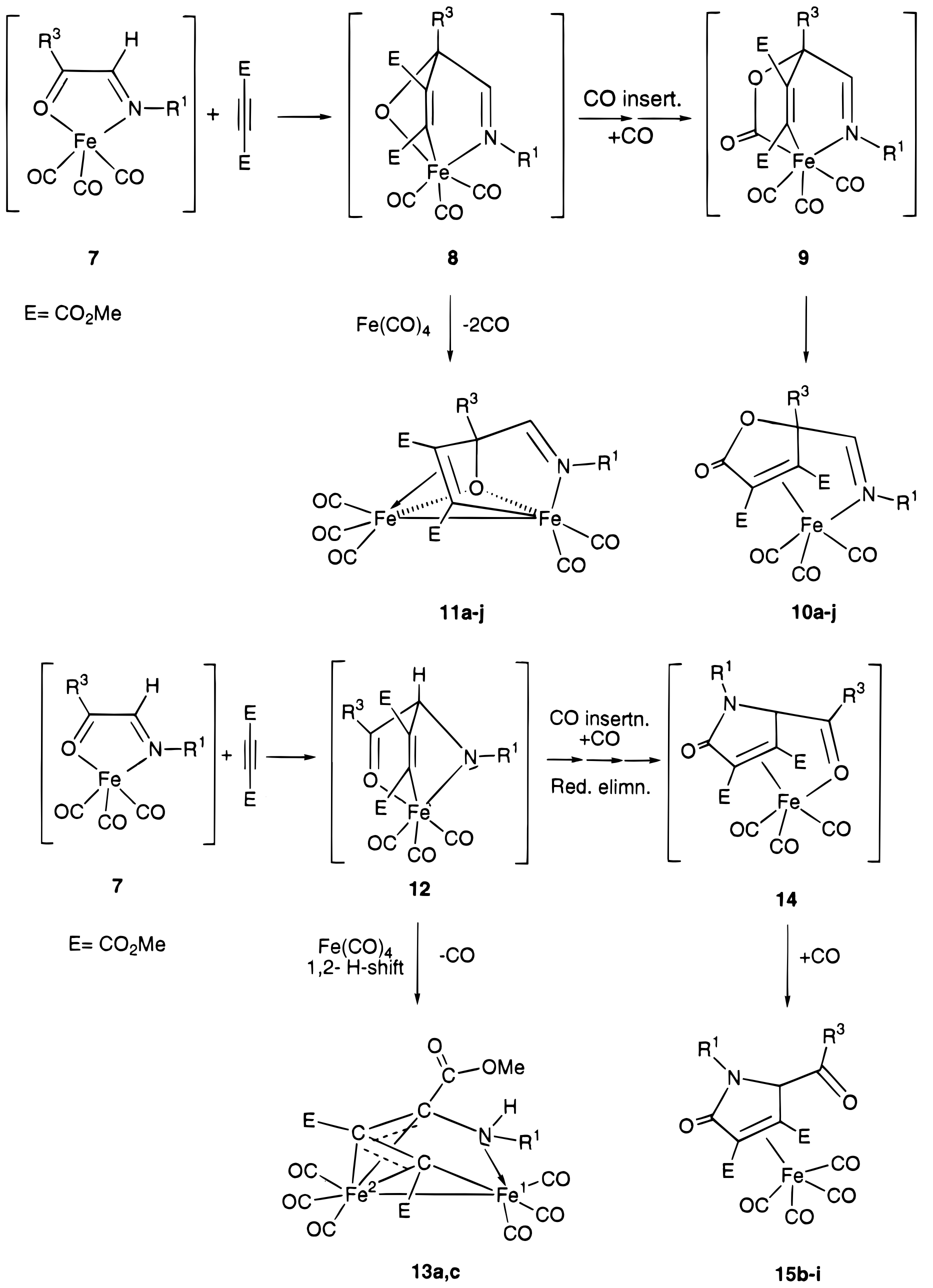

room temperature with MP to give the Fe(CO)$_3$(butenolide) complexes (**16f**,**i**) and the Fe(CO)$_3$(tricyclic) complexes (**20c**,**f**,**i**), as a result of an exclusive cycloaddition reaction to the Fe–O=C fragment (cf. Scheme 3). Similar complexes have been obtained in the reaction of Fe(CO)$_3$(α-imino ketone) with MP (cf. Scheme 1; **4** and **6**).[9] The ^{1}H and ^{13}C NMR data of complexes **16** and **20** both show only one set of resonances, which indicates that only one regioisomeric complex **16** and only one possible linkage isomer of complex **20** is formed. On the basis of the similarities with complexes **4** and **6**, complexes **16** and **20** are assigned to the analogous isomers; i.e., the ester-substituted alkyne (MP) carbon atom is C–C connected with the former ketone carbon atom of the α-imino ester. The tridentate heterocyclic ligand in **20** is formed from intermediate **18** via C–C coupling of the unsubstituted carbon of the π-coordinated MP (additional ligand) and the unsubstituted carbon of the π-coordinated butenolide C=C bond. Complexes **20** can also be prepared in almost quantitative yield by irradiation of **16** in the presence of excess MP. Irradiation of complexes **10c**,**f**,**i** (DMAD) in the presence of excess MP leads to the mixed Fe(CO)$_3$(tricyclic) complexes **19** in moderate yield. The presence of only one set of resonances in the ^{1}H and ^{13}C NMR indicates that again only one linkage isomer is formed. The X-ray molecular structure determination of **19c** showed that it is, as expected, the isomer in which the unsubstituted carbon atom of the MP fragment is C–C connected.

Decomplexation Reactions. When they are heated in THF, complexes **10c**–**j** lose their CO ligands. Subsequent reaction of the resulting intermediate with water at room temperature results in liberation of the N-protonated organic butenolide derivatives **21** (cf. Scheme 4).

Scheme 3. Reactions of Fe(CO)$_3$(α-iminoester) (7) and Fe(CO)$_3$(butenolide) (10/16) with MP

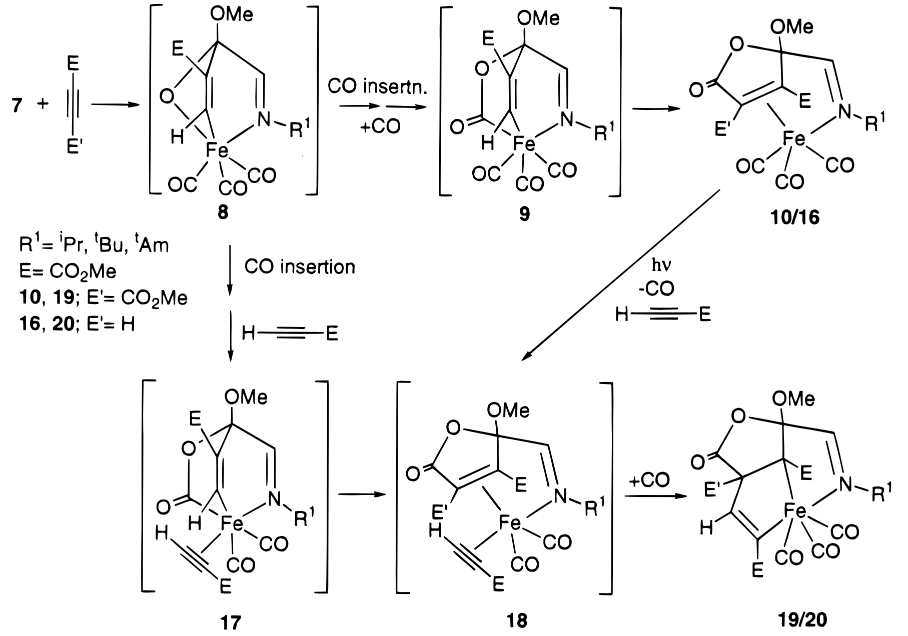

Scheme 4. Decomplexation Reactions of Fe(CO)$_3$(butenolide) (10)

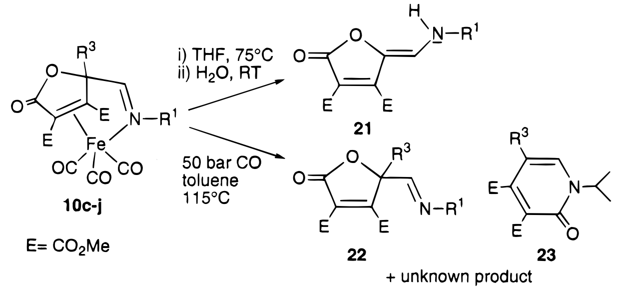

The molecular structure is confirmed by a single-crystal X-ray diffraction determination of **21c**. Reaction of **10f**−**j** under CO pressure (50 bar) at 115 °C results in the free butenolides (**22**) together with Fe(CO)$_5$. The butenolides **22f**−**j** are isolated in purities of ca. 90% and in high yields (80%), except for **22h** (30%), which is formed together with several side products. From complexes **10c**−**e**, under these reaction conditions, two new organic products are formed besides **21c**−**e**, of which one, a δ-lactam (**23c**−**e**), could be isolated.

Molecular Structure of Fe(CO)$_3$(butenolide) (10d). An ORTEP drawing of the molecular structure of **10d** together with the atomic numbering scheme is shown in Figure 1. Selected bond lengths and angles are given in Table 5.

The coordination around the central iron atom is distorted trigonal bipyramidal. As expected in a d^8-tbp complex, the imine nitrogen is axially coordinated and the C(8)−C(11) double bond occupies an equatorial position.[36] The largest deviation from a tbp geometry is observed for N(1)−Fe−C(15) (169.76(17)°), probably due to the steric interaction of the carbonyl C(15)−O(8) with the ester groups on C(8) and C(11). This is illustrated by the short distance C(15)···O(4) of 2.736(6) Å, which is 0.48 Å shorter than the sum of the van de Waals radii. A similar coordination geometry is found for the analogous complex Fe(CO)$_3$(butenolide) (**4**) (cf. Scheme 1; X = O, R^3 = Me, E = E′ = CO$_2$Me).[8] Because of their close structural resemblance, the solid-state structures will be compared. The Fe−N(1) bond distance of 2.017(3) Å is somewhat shorter than the Fe−N distance in **4** (2.055(2) Å), while the short intact imine bond (N(1)−C(4) = 1.266(5) Å) indicates that there is hardly any π-back-donation to the isolated imine fragment. The Fe−C(15), Fe−C(16), and Fe−C(17) distances are 1.796(5), 1.821(5), and 1.816(5) Å, respectively, normal Fe−CO distances. The comparatively short Fe−C(15) bond distance reflects the enhanced π-back-donation to this carbonyl due to the *trans*-positioned σ-donating imine nitrogen. The alkene double bond C(8)−C(11) is asymmetrically coordinated to iron (Fe−C(8) = 2.026(4) Å, Fe−C(11) = 2.082(4) Å), which is also observed in **4**, in **15h** (see below), and in many other π-coordinated alkene complexes.[37,38] The alkene double-

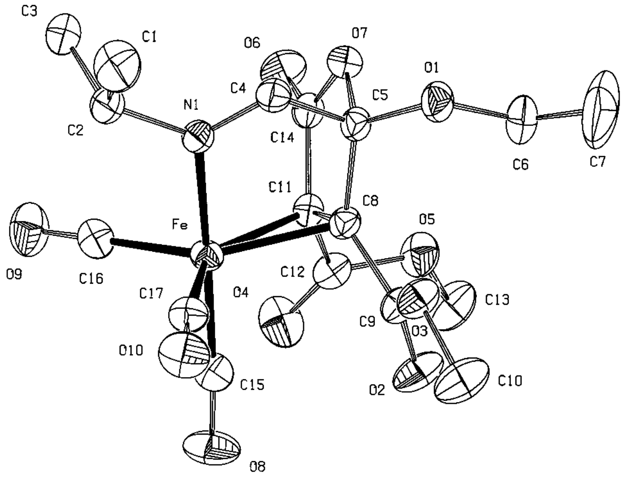

Figure 1. ORTEP drawing[34] (30% probability level) of the molecular structure of **10d**. Hydrogen atoms have been omitted for clarity.

---

(36) Rossi, A. R.; Hoffmann, R. *Inorg. Chem.* **1975**, *14*, 365.

(37) Whitesides, T. H.; Slave, R. W.; Calabrese, J. C. *Inorg. Chem.* **1974**, *13*, 1895.

Table 5. Selected Bond Distances (Å) and Angles (deg) for 10d (Esd's in Parentheses)

Fe−N(1)	2.017(3)	O(2)−C(9)	1.201(6)	O(7)−C(5)	1.462(5)	C(5)−C(8)	1.535(7)
Fe−C(8)	2.026(4)	O(3)−C(9)	1.340(6)	O(7)−C(14)	1.373(5)	C(8)−C(9)	1.482(6)
Fe−C(11)	2.082(4)	O(4)−C(12)	1.183(6)	N(1)−C(2)	1.488(6)	C(8)−C(11)	1.432(6)
Fe−C(15)	1.796(5)	O(5)−C(12)	1.324(6)	N(1)−C(4)	1.266(5)	C(11)−C(12)	1.523(7)
Fe−C(16)	1.821(5)	O(5)−C(13)	1.460(7)	C(4)−C(5)	1.493(6)	C(11)−C(14)	1.460(6)
Fe−C(17)	1.816(5)	O(6)−C(14)	1.197(5)				

N(1)−Fe−C(8)	82.83(17)	C(11)−Fe−C(16)	104.92(17)	O(1)−C(5)−C(4)	110.6(4)	O(2)−C(9)−O(3)	124.1(4)
N(1)−Fe−C(11)	97.65(16)	C(11)−Fe−C(17)	144.0(2)	O(1)−C(5)−C(8)	118.8(4)	O(2)−C(9)−C(8)	124.6(4)
N(1)−Fe−C(15)	169.76(17)	C(15)−Fe−C(16)	89.1(2)	O(7)−C(5)−C(4)	100.3(3)	O(3)−C(9)−C(8)	111.2(4)
N(1)−Fe−C(16)	95.30(19)	C(15)−Fe−C(17)	84.8(2)	O(7)−C(5)−C(8)	104.1(3)	C(8)−C(11)−C(12)	125.7(4)
N(1)−Fe−C(17)	84.99(18)	C(16)−Fe−C(17)	110.6(2)	C(4)−C(5)−C(8)	112.3(3)	C(8)−C(11)−C(14)	108.6(4)
C(8)−Fe−C(11)	40.74(16)	C(5)−O(7)−C(14)	110.4(3)	O(1)−C(6)−C(7)	109.7(7)	C(12)−C(11)−C(14)	112.6(4)
C(8)−Fe−C(15)	99.0(2)	Fe−N(1)−C(4)	117.6(3)	C(5)−C(8)−C(9)	123.6(4)	Fe−C(15)−O(8)	172.8(4)
C(8)−Fe−C(16)	144.10(18)	C(2)−N(1)−C(4)	120.6(4)	C(5)−C(8)−C(11)	106.0(4)	Fe−C(16)−O(9)	176.4(4)
C(8)−Fe−C(17)	105.0(2)	N(1)−C(4)−C(5)	114.8(4)	C(9)−C(8)−C(11)	125.5(4)	Fe−C(17)−O(10)	174.2(5)
C(11)−Fe−C(15)	90.14(19)	O(1)−C(5)−O(7)	108.8(3)				

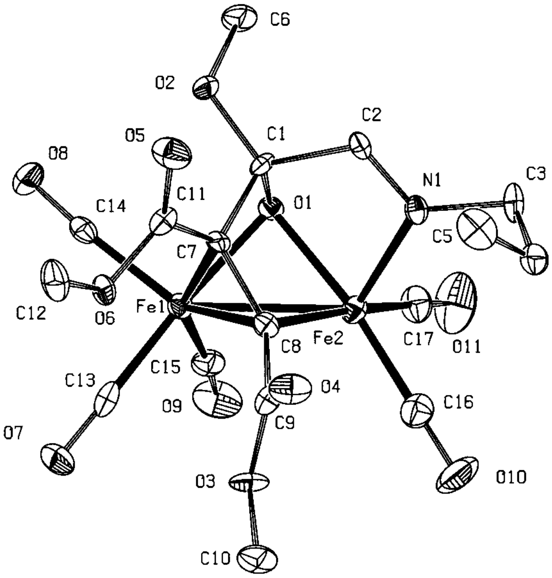

Figure 2. ORTEP drawing[34] (50% probability level) of the molecular structure of **11a**. Hydrogen atoms have been omitted for clarity.

bond distance of 1.432(6) Å is relatively long and lies between the values for single and double bonds. The elongation is probably not only a result of coordination to iron but also due to conjugation with the inserted carbonyl C(14)−O(6), which is reflected in the short C(14)−C(11) distance of 1.460(6) Å, and an almost perfect coplanarity (179.5(5)°) of these bonds. Furthermore, the relatively short C(8)−C(9) distance (1.482(6) Å) together with the torsion angle C(11)−C(8)−C(9)−O(2) bonds (0.0(3)°) suggests that there is additional conjugation with the carbonyl of the ester attached to C(8), which was also found in **4**.

Molecular Structure of $Fe_2(CO)_5$[*i*-PrN=C(H)C(OMe)(O)C(CO_2Me)=C(CO_2Me)] (11a). An ORTEP drawing of the molecular structure of **11a** together with the atomic numbering scheme is shown in Figure 2; selected bond distances and angles are given in Table 6.

The molecular structure of **11a** consists of an $Fe(CO)_3$ and an $Fe(CO)_2$ fragment (all CO ligands are terminally bonded with normal bond lengths and angles) held together by a metal−metal bond (Fe(1)−Fe(2) = 2.5257(10) Å) and a new bridging eight-electron-donating ligand. The new ligand results from C−C bond formation between one of the alkyne DMAD carbons (C(7)) and the former carboxy carbon atom C(1) of the α-imino ester. The formation of this type of ligand (with a bridging NR^1 moiety instead of the bridging oxygen O(1) in **11a**) has been observed earlier; i.e., reaction of RuM(CO)$_6$(R-DAB) (M = Ru, Fe)[39−41] with DMAD results in the comparable RuM(CO)$_6$(AIB)[42] complexes. In **11a** the olato oxygen O(1) is σ(O)-bonded to Fe(1) (Fe(1)−O(1) = 1.946(3) Å) and is also bonded to Fe(2) via a σ(O) donative bond (Fe(2)−O(1) = 1.942(3) Å), thus forming a nearly symmetrical Fe(1)−O(1)−Fe(2) bridge with an angle of 81.01(12)°.

Both the Fe−O distances and the Fe−O−Fe angle compare well with those found in $Fe_2(CO)_6$[C(Et)=C(Et)(CO_2)].[43] The ligand in **11a** is furthermore bonded to Fe(2) with a normal σ(N) donative bond (Fe(2)−N(1) = 1.966(4) Å) and an Fe−C bond with the former alkyne carbon C(8). The Fe(2)−C(8) bond distance of 1.944(5) Å compares well with the bond length of 1.955(5) Å found in the isostructural FeRu(CO)$_6$(AIB).[39] As a consequence of the C−C coupling, the alkyne bond C(7)−C(8) has become a double bond (C(7)−C(8) = 1.402(6) Å), which is elongated due to its π-coordination to Fe(1) (Fe(1)−C(7) = 2.129(4) Å, Fe(1)−C(8) = 2.053(4) Å). The asymmetric coordination of the alkene is also observed in FeRu(CO)$_6$(AIB),[39] which is probably due to the σ(C) bonding of C(8) to Fe(2).

Molecular Structure of $Fe_2(CO)_6$[*i*-PrN(H)C(CO_2Me)C(CO_2Me)C(CO_2Me)] (13c). An ORTEP drawing of the molecular structure of **13c** together with the atomic numbering scheme is shown in Figure 3. Selected bond lengths and angles are given in Table 7.

The molecular structure of **13c** consists of two inequivalent $Fe(CO)_3$ units, with all CO ligands terminally bonded with normal bond distances and angles, which are linked by a single Fe−Fe bond (Fe(1)−Fe(2) = 2.5671(17) Å) and bridged by a newly formed formally

---

(38) Enders, D.; Schmitz, T.; Raabe, G.; Krüger, C. *Acta Crystallogr.* **1991**, *C47*, 37 and references therein.

(39) Muller, F.; van Koten, G.; Kraakman, M. J. A.; Vrieze, K.; Zoet, R.; Duineveld, K. A. A.; Heijdenrijk, D.; Stam, C. H.; Zoutberg, M. C. *Organometallics* **1989**, *8*, 982.

(40) Muller, F.; Dijkhuis, D. I. P.; van Koten, G.; Vrieze, K.; Heijdenrijk, D.; Rotteveel, M. A.; Stam, C. H.; Zoutberg, M. C. *Organometallics* **1989**, *8*, 992.

(41) Staal, L. H.; van Koten, G.; Vrieze, K.; van Santen, B.; Stam, C. H. *Inorg. Chem.* **1981**, *20*, 3598.

(42) AIB(R^1,E,E′) is the abbreviation for the organic ligand resulting from C−C bond formation between an R-DAB ligand and the alkyne EC≡CE′. The backbone of the ligand is R^1N=C(H)C(H)(NR^1)C(E)=CE′, which is 3-amino-4-imino-1-butene.

(43) Aime, S.; Milone, L.; Sappa, E.; Tirpicchio, A.; Tirpicchio Camellini, M. *J. Chem. Soc., Dalton Trans.* **1979**, 1155.

Table 6. Selected Bond Distances (Å) and Angles (deg) for 11a (Esd's in Parentheses)

Fe(1)−Fe(2)	2.5257(10)	Fe(1)−C(15)	1.807(6)	O(1)−C(1)	1.432(6)	C(1)−C(2)	1.509(6)
Fe(1)−O(1)	1.946(3)	Fe(2)−O(1)	1.942(3)	O(2)−C(1)	1.383(5)	C(1)−C(7)	1.522(7)
Fe(1)−C(7)	2.129(4)	Fe(2)−N(1)	1.966(4)	O(4)−C(9)	1.202(6)	C(7)−C(8)	1.402(6)
Fe(1)−C(8)	2.053(4)	Fe(2)−C(8)	1.944(5)	O(5)−C(11)	1.202(7)	C(7)−C(11)	1.477(7)
Fe(1)−C(13)	1.778(5)	Fe(2)−C(16)	1.778(6)	N(1)−C(2)	1.273(7)	C(8)−C(9)	1.483(7)
Fe(1)−C(14)	1.828(5)	Fe(2)−C(17)	1.820(5)	N(1)−C(3)	1.465(6)		

Fe(1)−O(1)−Fe(2)	81.01(12)	C(2)−N(1)−C(3)	119.9(5)	C(2)−C(1)−C(7)	112.1(4)	C(7)−C(8)−C(9)	121.9(4)
Fe(1)−O(1)−C(1)	98.5(2)	O(1)−C(1)−O(2)	111.2(3)	N(1)−C(2)−C(1)	113.6(5)	Fe(1)−C(13)−O(7)	176.8(4)
Fe(2)−O(1)−C(1)	101.5(2)	O(1)−C(1)−C(2)	104.5(4)	C(1)−C(7)−C(8)	109.8(4)	Fe(1)−C(14)−O(8)	175.1(5)
C(1)−O(2)−C(6)	113.2(4)	O(1)−C(1)−C(7)	100.6(3)	C(1)−C(7)−C(11)	120.6(4)	Fe(1)−C(15)−O(9)	173.9(4)
Fe(2)−N(1)−C(2)	111.4(3)	O(2)−C(1)−C(2)	115.2(4)	C(8)−C(7)−C(11)	124.7(4)	Fe(2)−C(16)−O(10)	179.3(6)
Fe(2)−N(1)−C(3)	128.8(4)	O(2)−C(1)−C(7)	112.0(4)	Fe(1)−C(8)−Fe(2)	78.33(17)	Fe(2)−C(17)−O(11)	178.4(5)

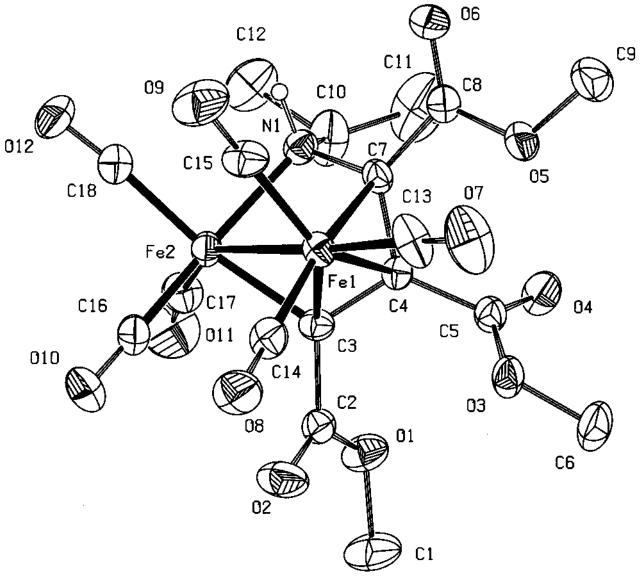

Figure 3. ORTEP drawing[34] (30% probability level) of the molecular structure of **13c**. Hydrogen atoms, except for the amine N(1)−H, have been omitted for clarity.

dianionic eight-electron-donating ligand. The ligand results from coupling of the former alkyne carbon C(4) to the former imine carbon C(7) followed by an 1,2-H shift of the imine proton to nitrogen, resulting in an allyl−amine type of ligand which is $\mu_2,\sigma(N):\eta^3$-$R^1N(H)C(E)C(E)C(E)$ (E = CO_2Me) coordinated. A similar type of coordination has been observed in $Fe_2(CO)_6[HCC(C(O)CH_3)C(O)CH_3)S$-*t*-Bu][44] and $Ru_2(CO)_6[CH_3CC(H)C(H)N{=}C(CH_3)_2]$.[45] The C(7)−C(4)−C(3) fragment is η^3-allyl coordinated to the $Fe(1)CO_3$ unit (Fe(1)−C(7) = 2.083(5) Å, Fe(1)−C(4) = 2.053(5) Å, Fe(1)−C(3) = 2.020(6) Å, C(7)−C(4) = 1.429(8) Å, C(4)−C(3) = 1.398(8) Å), with the outer allylic carbon C(3) also σ-bonded to Fe(2): i.e., bridging between the two metal centers.

The Fe(2)−C(3) bond distance of 1.965(6) Å is within the range generally observed for Fe−C(sp^2) bonds.[46−49] The Fe−C bond distances in the allyl part are almost identical with those observed for $Fe_2(CO)_6[HCC(C(O)CH_3)C(O)CH_3)S$-*t*-Bu][44] and are on average 0.10 Å shorter than in $Ru_2(CO)_6[CH_3CC(H)C(H)N{=}C(CH_3)_2]$,[45] which is expected due to the smaller covalent radius of Fe. The new amine fragment is σ(N)-coordinated to Fe(2) at a distance of 2.064(5) Å, comparable to the Fe−N bond distance of 2.030(8) Å found in the isostructural complex $Fe_2(CO)_5[i$-$PrNCHCHN(i$-$Pr)C(O)C(Me){=}CNEt_2]$.[50] The reduction of the imine to an amine is expressed by the N(1)−C(7) bond distance of 1.464(8) Å. A hydrogen bond, donated from N(1) toward O(6) [1 − *x*, 1 − *y*, 2 − *z*], with N···O = 3.203(8) Å and N−H···O = 171.4(6)°, forms dimers of **13c** in the crystal.

Molecular Structure of $Fe(CO)_4(\pi$-pyrrolinone) (15h). An ORTEP drawing of the molecular structure of **15h** together with the atomic numbering scheme is shown in Figure 4; selected bond distances and angles are given in Table 8.

As expected, the coordination geometry around the central iron atom is distorted trigonal bipyramidal with the double bond C(5)−C(6) of the pyrrolinone ligand π-coordinated in an equatorial position.[36] Similar coordination geometries have been observed in several π-coordinated $Fe(CO)_4(\eta^2$-alkene) complexes.[37,38,51] Furthermore, the molecular structure of **15h** is closely related to the solid-state structure of $Fe(CO)_3$(1,5-dihydropyrrol-2-one)[3] (**4**) (cf. Scheme 1; X = N-*i*-Pr, R^3 = H, E = E′ = CO_2Me), except for the coordinated imine. The alkene double bond C(5)−C(6) is asymmetrically coordinated (Fe(1)−C(5) = 2.099(4) Å, Fe(1)−C(6) 2.045(4) Å) to the iron, as in **4** and **10d** (see above). This feature is probably due to steric interactions of the pyrrolinone ligand with the terminal CO ligands. The Fe(1)−C(alkene) bond lengths compare well with those found for other $Fe(CO)_4(\eta^2$-alkene) complexes.[37,38] The alkene double-bond distance (C(5)−C(6) = 1.435(5) Å) indicates a substantial reduction of the bond order, due to π-back-donation from the Fe(0) atom into the antibonding π* alkene orbital. The alkene bond distance, and the other bond distances within the five-membered pyrrolinone ring in **15h**, are comparable with those found in **4**. As expected for an η^2-coordinated alkene, the ester substituents on the alkene carbons C(5) and C(6) are bent away from the metal center by 23° and 27°.

Molecular Structure of the Tricyclic Compound 19c. An ORTEP drawing of the molecular structure of **19c** together with the atomic numbering scheme is shown in Figure 5; selected bond distances and angles are given in Table 9.

---

(44) Seyferth, D.; Hoke, J. B.; Dewan, J. C. *Organometallics* **1987**, *6*, 895.

(45) Mul, W. P.; Elsevier, C. J.; Vrieze, K.; Smeets, W. J. J.; Spek, A. L. *Organometallics* **1992**, *11*, 1891.

(46) Muller, F.; van Koten, G.; Vrieze, K.; Heijdenrijk, D. *Inorg. Chim. Acta* **1989**, *158*, 69.

(47) Kisch, H.; Krüger, C.; Marcolin, H. E.; Trautwein, A. X. *Z. Naturforsch.* **1987**, *42B*, 1435.

(48) Lindner, E.; Krieg, C.-L.; Hiller, W.; Fawzi, R. *Angew. Chem.* **1984**, *96*, 508.

(49) Birk, R.; Grössmann, U.; Hund, H.-U.; Berke, H. *J. Organomet. Chem.* **1988**, *345*, 321.

(50) Muller, F.; van Koten, G.; Kraakman, M. J. A.; Vrieze, K.; Heijdenrijk, D.; Zoutberg, M. C. *Organometallics* **1989**, *8*, 1331.

(51) tom Dieck, H.; Diercks, R.; Stamp, L.; Bruder, H.; Schuld, T. *Chem. Ber.* **1987**, *120*, 1943.

Table 7. Selected Bond Distances (Å) and Angles (deg) for 13c (Esd's in Parentheses)

Fe(1)−Fe(2)	2.5671(17)	Fe(1)−C(15)	1.795(7)	O(2)−C(2)	1.207(8)	C(2)−C(3)	1.479(9)
Fe(1)−C(3)	2.020(6)	Fe(2)−N(1)	2.064(5)	O(4)−C(5)	1.209(8)	C(3)−C(4)	1.398(8)
Fe(1)−C(4)	2.053(5)	Fe(2)−C(3)	1.965(6)	O(6)−C(8)	1.203(9)	C(4)−C(5)	1.492(9)
Fe(1)−C(7)	2.083(5)	Fe(2)−C(16)	1.785(8)	N(1)−C(7)	1.464(8)	C(4)−C(7)	1.429(8)
Fe(1)−C(13)	1.834(8)	Fe(2)−C(17)	1.789(8)	N(1)−C(10)	1.540(11)	C(7)−C(8)	1.484(9)
Fe(1)−C(14)	1.794(7)	Fe(2)−C(18)	1.817(9)				
Fe(2)−N(1)−C(7)	100.4(3)	Fe(1)−C(3)−C(4)	71.2(3)	C(3)−C(4)−C(7)	111.1(5)	Fe(1)−C(7)−C(8)	114.8(5)
Fe(2)−N(1)−C(10)	116.3(5)	Fe(2)−C(3)−C(2)	124.2(4)	C(5)−C(4)−C(7)	125.6(5)	N(1)−C(7)−C(4)	113.5(5)
C(7)−N(1)−C(10)	112.0(5)	Fe(2)−C(3)−C(4)	112.8(4)	Fe(1)−C(7)−N(1)	105.4(4)	N(1)−C(7)−C(8)	116.6(5)
Fe(1)−C(3)−Fe(2)	80.2(2)	C(2)−C(3)−C(4)	121.2(5)	Fe(1)−C(7)−C(4)	68.7(3)	C(4)−C(7)−C(8)	125.7(6)
Fe(1)−C(3)−C(2)	128.4(5)	C(3)−C(4)−C(5)	123.2(5)				

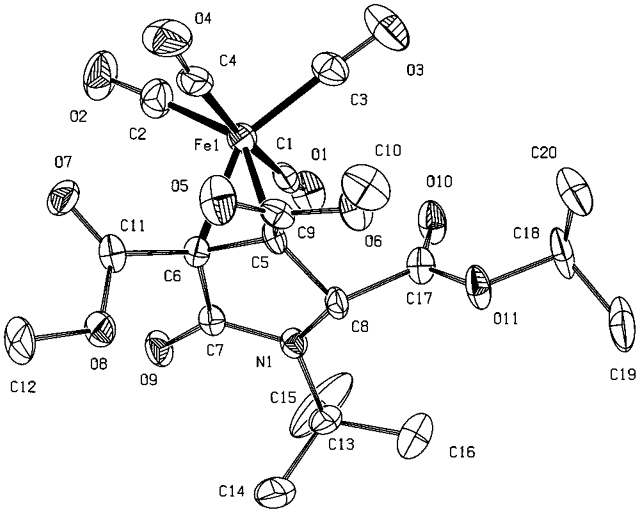

Figure 4. ORTEP drawing[34] (50% probability level) of the molecular structure of **15h**. Hydrogen atoms have been omitted for clarity.

The central iron atom in **19c** has a slightly distorted octahedral coordination geometry and is coordinated by a dianionic tridentate ligand. A similar arrangement has been observed for the isostructural tricyclic complex **6** (cf. Scheme 1; X = N-*t*-Bu, R^3 = Me),[9] which is formed in the reaction of $Fe(CO)_3$(α-imino ketone) with 2 equiv of MP. Because of the structural resemblance of **19c** and **6**, their solid-state structures will be compared. The intact imine (N(1)−C(7) = 1.268(2) Å) at the 2-position of the lactone ring is coordinated to iron with a normal σ(N) donative bond (Fe(1)−N(1) = 2.0283(18) Å), which is somewhat shorter than in **6** (2.0499(16) Å). The olefinic part C(18)−C(17) on the 4-position and the former alkyne atom C(14) are both covalently bound to iron, thus forming a tricyclic structure. The Fe(1)−C(18) (2.0059(19) Å) bond distance compares well with that found in **6** (2.0045(18) Å), whereas the Fe(1)−C(14) bond distance (2.0642(17) Å) is significantly shorter (2.1129(17) Å), but they are both consistent with comparable Fe−C(sp^2)[46−49,51] and Fe−C(sp^3)[52−56] distances reported in the literature. The angles within the backbone of the ligand reveal that there is no strain, which, together with the observed octahedral geometry, shows that the ligand is well-suited to span three facial coordination sites; i.e., all three atoms are coordinated *trans* to a CO ligand. The increased π-back-donation to the carbonyl *trans* to the σ-donating imine nitrogen is expressed by the relatively short Fe(1)−C(3) (1.7791(14) Å) bond length. The former butenolide double bond C(11)−C(14) is, as a consequence of the C−C coupling with the alkyne carbon C(17), reduced to a single bond (1.559(3) Å), while the former alkyne bond (C(17)−C(18)) is elongated to 1.325(3) Å, a normal double-bond distance.

Molecular Structure of Butenolide 21c. An ORTEP drawing of **21c** together with the atomic numbering scheme is shown in Figure 6; the selected bond distances and angles are given in Table 10.

The bond distances within the butenolide C(8)−O(6)−C(1)−C(2)-C(5) ring vary between 1.434(2) and 1.384(2) Å, which is indicative of a delocalized system. Also interesting are the bond lengths and angles within the enamine unit. The formal double bond (C(8)−C(9) = 1.387(2) Å) is elongated compared to the mean value of 1.34 Å for a double bond, and the amine bond (N(1)−C(9) = 1.305(2) Å) is significantly shortened compared to the mean value of 1.40 Å for a normal amine bond. Furthermore, the sum of the bond angles around N(1) (H(1) is found and refined) is 360(2)°, which is indicative of sp^2 hybridization. The angle N(1)−C(9)−C(8) of 123.17° is also indicative of sp^2 hybridization. (Also, the sum of the angles involving C(9) is 360.0(3)°; however, H(9) is placed on a calculated position.) All this can be explained by a full conjugation of the nitrogen lone pair and the C(8)−C(9) double bond (enamine unit), and the butenolide ring (see Scheme 5). This is corroborated by the planarity (±0.01 Å) of the C(8)−O(6)−C(1)−C(2)−C(5) ring, with C(9) and N(1) only 0.0941(16) and 0.2174(14) Å from this plane. The relatively short C(2)−C(3) distance (1.456(2) Å) and the relatively long carbonyl distance (1.206(2) Å) together with the torsion angle C(5)−C(2)−C(3)−O(2) of −20.3(2)° suggest, furthermore, some additional conjugation with this ester group. The amine nitrogen atom H(1) is involved in a bifurcated hydrogen bond toward O(6) (intramolecular with N(1)···O(6) = 2.737(2) Å, N(1)−H(1)···O(6) = 101.9(15)°) and intermolecular toward O(1) (1 − *x*, −*y*, −*z*; N(1)···O(1) = 2.779(2) Å, N(1)−H(1)···O(1) = 156.0(20)°); the sum of the angles involving the hydrogen atom amounts to 359.6(27)°, which is in accordance with the bifurcated nature of the hydrogen bonding system. The intermolecular hydrogen bond links **21c** into dimers.

IR Spectroscopy. The IR data for the complexes **10**, **11**, **13**, **15**, **16**, and **19**−**23** are collected in Table 11 together with the FD-mass data and the elemental analyses.

Complexes 10a−j. The three terminal CO ligands in **10a−j** give rise to a characteristic absorption pattern, a sharp absorption around 2070 cm^{-1} and two partially

---

(52) Eilbracht, P.; Jelitte, R.; Walz, L. *Chem. Ber.* **1984**, *117*, 3473.

(53) Grevels, F.-W.; Feldhoff, U.; Leitich, J.; Krüger, C. *J. Organomet. Chem.* **1974**, 79.

(54) Krüger, C.; Tsay, Y.-H. *Cryst. Struct. Commun.* **1975**, *5*, 215.

(55) Lindner, E.; Schauss, E.; Hiller, W.; Fawzi, R. *Angew. Chem.* **1984**, *96*, 727.

(56) de Lange, P. P. M.; van Wijnkoop, M.; Frühauf, H.-W.; Vrieze, K.; Goubitz, K. *Organometallics* **1993**, *12*, 428.

Table 8. Selected Bond Distances (Å) and Angles (deg) for 15h (Esd's in Parentheses)

Fe(1)−C(1)	1.833(5)	Fe(1)−C(6)	2.045(4)	N(1)−C(7)	1.369(6)	C(5)−C(9)	1.473(7)
Fe(1)−C(2)	1.811(5)	O(5)−C(9)	1.200(7)	N(1)−C(8)	1.458(6)	C(6)−C(7)	1.509(6)
Fe(1)−C(3)	1.808(5)	O(7)−C(11)	1.194(6)	N(1)−C(13)	1.505(7)	C(6)−C(11)	1.507(6)
Fe(1)−C(4)	1.823(6)	O(9)−C(7)	1.217(5)	C(5)−C(6)	1.435(5)	C(8)−C(17)	1.532(7)
Fe(1)−C(5)	2.099(4)	O(10)−C(17)	1.197(7)	C(5)−C(8)	1.529(7)		
C(1)−Fe(1)−C(2)	86.9(2)	C(2)−Fe(1)−C(6)	101.7(2)	C(7)−N(1)−C(13)	121.2(4)	O(9)−C(7)−N(1)	127.1(5)
C(1)−Fe(1)−C(3)	87.4(2)	C(3)−Fe(1)−C(4)	88.6(2)	C(8)−N(1)−C(13)	123.9(4)	O(9)−C(7)−C(6)	124.8(4)
C(1)−Fe(1)−C(4)	169.3(2)	C(3)−Fe(1)−C(5)	103.8(2)	C(6)−C(5)−C(9)	121.5(4)	N(1)−C(7)−C(6)	108.0(3)
C(1)−Fe(1)−C(5)	99.0(2)	C(3)−Fe(1)−C(6)	144.1(2)	C(8)−C(5)−C(9)	117.6(4)	N(1)−C(8)−C(5)	103.7(4)
C(1)−Fe(1)−C(6)	94.44(17)	C(4)−Fe(1)−C(5)	91.6(2)	C(5)−C(6)−C(7)	106.8(4)	N(1)−C(8)−C(17)	113.6(4)
C(2)−Fe(1)−C(3)	114.2(2)	C(4)−Fe(1)−C(6)	94.7(2)	C(5)−C(6)−C(11)	125.3(4)	C(5)−C(8)−C(17)	113.1(4)
C(2)−Fe(1)−C(4)	85.7(2)	C(5)−Fe(1)−C(6)	40.49(15)	C(7)−C(6)−C(11)	115.0(3)	O(11)−C(18)−C(19)	107.1(4)
C(2)−Fe(1)−C(5)	141.8(2)	C(7)−N(1)−C(8)	112.4(4)				

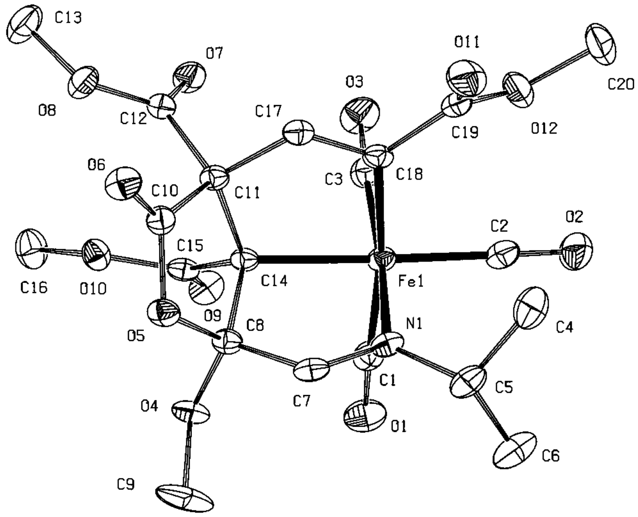

Figure 5. ORTEP drawing[34] (50% probability level) of the molecular structure of **19c**. Hydrogen atoms have been omitted for clarity.

resolved bands between 2015 and 1990 cm^{-1}. The pattern and band positions in these spectra closely resemble those of the analogous Fe(CO)$_3$(butenolide)[8] complexes **4** (cf. Scheme 1; X = O) derived from cycloaddition of Fe(CO)$_3$(α-imino ketone) with DMAD. As in the latter complexes, three separate absorptions are observed in the organic carbonyl region between 1761 and 1699 cm^{-1}. The high-frequency absorption (around 1760 cm^{-1}) is assigned to the lactone carbonyl because the carbonyl stretching bands of unsaturated four- and five-membered cyclic carbonyls are generally observed at frequencies higher than those of open-chain ester carbonyl groups due to ring strain.[57] The other two bands are consequently assigned to the carbonyls of the ester groups.

Complexes 11a,f. The terminal CO ligands in complexes **11** give rise to an absorption pattern which is characteristic for this type of complex. The pattern and position of these bands closely resemble those observed for the closely related Fe$_2$(CO)$_5$(OIB)[22,58] and Fe$_2$(CO)$_5$(OPP)[58,59] complexes, which are shown in Chart 1 (derived from the in situ cycloaddition reactions of the α-imino ketones, R^{1}N═C(R^2)C(R^3)═O (R^1 = *p*-Tol, *t*-Am, R^2 = H, Ph, R^3 = Me, Ph) and C$_5$H$_4$N-2-C(R^3)═O (R^3 = H, Me, Ph) with DMAD, respectively) and that of complex **25** (cf. Scheme 8).

Although in these complexes the σ,π-coordination of the former alkyne is generally opposite to that observed in **11**, this does not change the pattern of the CO stretching bands. The two ester groups of the former alkyne give rise to two separate absorptions at 1735 and 1705 cm^{-1}.

Complexes 13a,c. The six terminal CO ligands in the new complexes **13** in hexane give rise to five absorptions in the ν(CO) region (**13c**; 2077 (s), 2039 (vs), 2010 (s), 1998 (s), and 1992 cm^{-1}). The spectrum closely resembles that found for the comparable Fe$_2$(CO)$_6$[HCC-(C(O)CH$_3$)C(O)CH$_3$)S-*t*-Bu][44] complex. However, due to the low solubility of **13** in hexane the N−H absorption could not be observed. Therefore, the spectra are recorded in CH$_2$Cl$_2$, giving rise to four absorptions in the ν(CO) region between 2077 and 1997 cm^{-1}. The new N−H bonds in **13a**,**c** give rise to absorptions in the ν-(NH) region at 3266 and 3259 cm^{-1}, respectively. The positions of these N−H absorptions compare well to those found for Fe(CO)$_2$(σ(*N*): σ(*C*)-*i*-PrN(**H**)C(H)CR^3)$_2$[35] and are in general somewhat lower than those observed (3275−3302 cm^{-1}) for FeM(CO)$_6$[RNC(R)C(R)N(**H**)R][60] (M = Mn, Re) and the isostructural Ru$_2$(CO)$_6$[RCC(H)C-(H)N(**H**)R].[61] The ester carbonyl groups give rise to two weak absorptions in the organic carbonyl region.

Complexes 15f−h. Complexes **15** show a characteristic CO absorption pattern with bands around 2112, 2047, and 2017 cm^{-1}. The pattern and position of these absorption bands are characteristic for equatorially substituted Fe(CO)$_4$(L) complexes[62] and closely resemble those observed for several other Fe(CO)$_4$(η^2-alkene) complexes.[63−65] The broad band at ca. 1700 cm^{-1} in the organic carbonyl region is assigned to the ester groups of the coordinated alkyne. The absorption at higher frequency (1744−1733 cm^{-1}) is assigned to the ester of the former α-imino ester ligand, because this band shifts to lower frequency going from the methyl via the ethyl to the isopropyl ester fragment (**f**−**h**), a trend which is also observed in the free ligand.[35]

---

(57) Hesse, M.; Meier, H.; Zeeh, B. *Spectroscopic Methods in Organic Chemistry*; Georg Thieme Verlag: Stuttgart, New York, 1984.

(58) Siebenlist, R.; Frühauf, H.-W.; Vrieze, K.; Veldman, N.; Spek, A. L. To be submitted for publication.

(59) OPP(R^3) is the abbreviation for the organic ligand resulting from C−C bond formation between an C$_5$H$_4$N-2-C(R$_3$)═O and an alkyne EC≡CE (E = CO$_2$Me). The backbone of the ligand is C$_5$H$_4$N-2-C(R^3)-(O)C(E)═CE, which is 2-pyridinopropen-2-olato.

(60) Keijsper, K.; Mul, J.; van Koten, G.; Vrieze, K.; Ubbels, H. C.; Stam, C. H. *Organometallics* **1984**, *3*, 1732.

(61) Mul, W. P.; Elsevier, C. J.; van Leijen, M.; Vrieze, K.; Smeets, W. J. J.; Spek, A. L. *Organometallics* **1992**, *11*, 1877.

(62) Darensbourg, D. J.; Nelson, H. H.; Hyde, C. L. *Inorg. Chem.* **1974**, *13*, 2135.

(63) Hopman, J. C. P.; Hiemstra, H.; Speckamp, W. N. *J. Chem. Soc., Chem. Commun.* **1995**, 617.

(64) Whitesides, T. H.; Slaven, R. W. *J. Organomet. Chem.* **1974**, *67*, 99.

(65) Weiss, E.; Stark, K.; Lancaster, J. E.; Murdock, H. D. *Helv. Chim. Acta* **1963**, *27*, 288.

Table 9. Selected Bond Distances (Å) and Angles (deg) for 19c (Esd's in Parentheses)

Fe(1)−N(1)	2.0283(18)	Fe(1)−C(18)	2.0059(19)	N(1)−C(5)	1.495(3)	C(11)−C(14)	1.559(3)
Fe(1)−C(1)	1.8374(19)	O(5)−C(8)	1.459(2)	N(1)−C(7)	1.268(2)	C(11)−C(17)	1.508(2)
Fe(1)−C(2)	1.822(2)	O(5)−C(10)	1.359(2)	C(7)−C(8)	1.505(3)	C(14)−C(15)	1.526(3)
Fe(1)−C(3)	1.7791(19)	O(6)−C(10)	1.194(2)	C(8)−C(14)	1.536(3)	C(17)−C(18)	1.325(3)
Fe(1)−C(14)	2.0642(18)	C(10)−C(11)	1.531(3)	C(11)−C(12)	1.534(3)	C(18)−C(19)	1.483(3)
N(1)−Fe(1)−C(1)	91.04(8)	C(3)−Fe(1)−C(14)	89.91(8)	O(5)−C(8)−C(7)	105.40(14)	C(14)−C(11)−C(17)	108.00(14)
N(1)−Fe(1)−C(2)	97.59(8)	C(3)−Fe(1)−C(18)	84.96(8)	O(5)−C(8)−C(14)	107.78(14)	Fe(1)−C(14)−C(8)	106.30(12)
N(1)−Fe(1)−C(3)	170.28(8)	C(14)−Fe(1)−C(18)	81.46(7)	C(7)−C(8)−C(14)	111.93(15)	Fe(1)−C(14)−C(11)	112.68(12)
N(1)−Fe(1)−C(14)	83.62(7)	C(8)−O(5)−C(10)	110.67(14)	O(5)−C(10)−O(6)	120.87(17)	Fe(1)−C(14)−C(15)	115.79(12)
N(1)−Fe(1)−C(18)	86.91(7)	Fe(1)−N(1)−C(5)	129.14(13)	O(5)−C(10)−C(11)	110.16(15)	C(8)−C(14)−C(11)	102.36(14)
C(1)−Fe(1)−C(2)	90.74(9)	Fe(1)−N(1)−C(7)	115.43(14)	O(6)−C(10)−C(11)	128.90(17)	C(8)−C(14)−C(15)	107.66(15)
C(1)−Fe(1)−C(3)	96.30(8)	C(5)−N(1)−C(7)	115.43(18)	C(10)−C(11)−C(12)	113.90(15)	C(11)−C(14)−C(15)	110.92(15)
C(1)−Fe(1)−C(14)	90.72(8)	Fe(1)−C(18)−C(17)	118.08(13)	C(10)−C(11)−C(14)	105.15(15)	C(11)−C(17)−C(18)	118.65(17)
C(1)−Fe(1)−C(18)	172.08(8)	O(4)−C(8)−O(5)	109.79(14)	C(10)−C(11)−C(17)	109.60(15)	Fe(1)−C(18)−C(19)	126.21(14)
C(2)−Fe(1)−C(3)	88.70(9)	O(4)−C(8)−C(7)	111.74(15)	C(12)−C(11)−C(14)	112.19(15)	C(17)−C(18)−C(19)	115.71(17)
C(2)−Fe(1)−C(14)	178.09(8)	O(4)−C(8)−C(14)	110.01(14)	C(12)−C(11)−C(17)	107.85(15)	N(1)−C(7)−C(8)	118.21(17)
C(2)−Fe(1)−C(18)	97.11(8)						

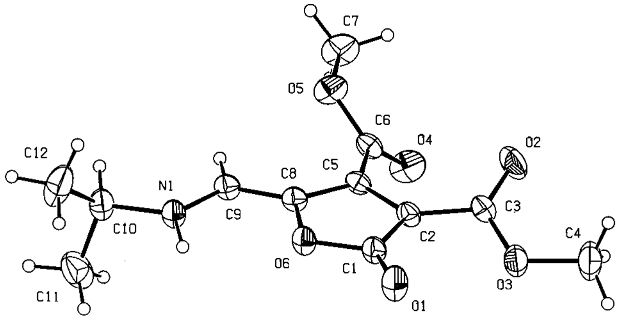

Figure 6. ORTEP drawing[34] (30% probability level) of the molecular structure of **21c**.

Complexes 16f,i. The pattern of the CO stretching bands of complexes **16** closely resembles those of complexes **10**, except for the shift of approximately 10 cm^{-1} to lower frequency as a result of the substitution of an electron-withdrawing ester group for a proton. In the organic carbonyl region two absorptions are observed. The one at higher frequency (1750 cm^{-1}) is, analogous to **10**, assigned to the lactone carbonyl. The other band is consequently assigned to the carbonyl of the ester fragment.

Complexes 19 and 20. The IR spectra of complexes **19** and **20** give rise to similar absorption patterns in the terminal ν(CO) region, except that the bands of complexes **19** are observed at somewhat higher frequency (10 cm^{-1}). This is probably due to the extra electron-withdrawing ester substituent present in **19**. The pattern and position of these spectra compare well with those of the isostructural tricyclic complexes **6** (cf. Scheme 1),[9] derived from reaction of Fe(CO)$_3$(α-imino ketone) with an excess of MP. In comparison to complexes **10** and **16**, the CO stretching bands are shifted to higher frequency due to the formal change of the oxidation state of the central iron from Fe(0) to Fe(II), which results in a decrease of π-back-donation. In the organic carbonyl region three absorptions are observed for complexes **19** and two for complexes **20**, although four and three carbonyl groups are present, respectively. The high-frequency band (1780−1800 cm^{-1}) in **19** and **20** is assigned to the cyclic ester carbonyl, as in **6**, **10**, and **16**. Analogous to complexes **6**, the absorptions of two ester carbonyl groups in both **19** and **20** coincide by chance, thus giving rise either to two bands at ca. 1735 and 1700 cm^{-1} (**19**) or to one band at ca. 1693 cm^{-1} (**20**).

Compounds 21. The new N−H bond in compounds **21** in CH$_2$Cl$_2$ gives rise to a weak absorption in the ν(NH) region between 3363 and 3368 cm^{-1}. In KBr, ν(NH) is observed as a very broad absorption around 3442 cm^{-1}. The rather large shift to higher frequency is probably due to the inter- and intramolecular hydrogen bridges present in the solid state, which are also observed in the X-ray structure of **21c**. The two ester carbonyl groups give rise to a broad and strong absorption around 1738 cm^{-1}, and the lactone carbonyl absorption is observed as a shoulder at ca. 1710 cm^{-1}. The shift to lower frequency of the lactone carbonyl compared to those in complexes **10** is probably due to delocalization of the negative charge (cf. Scheme 5). The absorption at 1650 cm^{-1} is assigned to the enamine fragment.

NMR Spectroscopy. The ^{1}H and ^{13}C NMR data of complexes **10**, **11**, **13**, **15**, **16**, and **19**−**23** are collected in Tables 12 and 13, respectively.

Complexes 10 and 16. The ^{1}H and ^{13}C NMR data of complexes **10** and **16** in solution are in agreement with the structure in the solid state (**10d**) and closely resemble those of the Fe(CO)$_3$(butenolide) complexes **4** (cf. Scheme 1; X = O, R^3 = Me, Ph). The imine proton resonances of **10** and **16** are observed between 7.83 and 7.60 ppm, which is indicative of an unchanged N=CH fragment. As a result of the C−C coupling, the ester methyl protons of the former alkyne in **10** are inequivalent and give rise to two separate resonances between 3.71 and 3.89 ppm and those of **16f**,**i** resonate at 3.74 and 3.78 ppm, respectively. The methoxy proton resonances of the R^3 substituent of ligands **a**−**c**,**f**,**i** are observed at slightly lower frequency (3.40−3.49 ppm). The alkene proton resonances in **16f**,**i**, observed as singlets at 4.05 and 4.08 ppm, are close to the resonances found at 4.18 and 4.08 ppm for the analogous complexes **4** and are within the range normally observed for protons on a coordinated alkene. The imine carbon atom resonances are observed between 183.6 and 176.2 ppm, which shows that the imine fragment is intact. The imine carbon resonances are shifted ca. 17 ppm to higher frequency compared to the free ligand, indicating that there is hardly any π-back-donation to the isolated imine fragment. This is corroborated by the short N=C distance (1.266(5) Å) in the solid-state structure of **10d**. The most pronounced changes in chemical shift are observed for carbon atoms directly involved in the C−C coupling reaction. The resonances of the former carboxy

Table 10. Selected Bond Distances (Å) and Angles (deg) for 21c (Esd's in Parentheses)

O(1)−C(1)	1.218(2)	O(6)−C(8)	1.3865(18)	C(1)−C(2)	1.434(2)	C(5)−C(6)	1.499(2)
O(2)−C(3)	1.206(2)	N(1)−C(9)	1.305(2)	C(2)−C(3)	1.456(2)	C(5)−C(8)	1.384(2)
O(4)−C(6)	1.189(2)	N(1)−C(10)	1.465(3)	C(2)−C(5)	1.390(2)	C(8)−C(9)	1.387(2)
O(6)−C(1)	1.386(2)	N(1)−H(1)	0.98(2)				
C(1)−O(6)−C(8)	108.14(11)	C(1)−C(2)−C(3)	124.69(14)	C(2)−C(5)−C(6)	126.14(13)	O(6)−C(8)−C(5)	109.20(13)
C(9)−N(1)−C(10)	125.15(14)	C(1)−C(2)−C(5)	107.18(13)	C(2)−C(5)−C(8)	108.09(12)	O(6)−C(8)−C(9)	117.14(13)
O(1)−C(1)−O(6)	119.49(14)	C(3)−C(2)−C(5)	127.96(13)	C(6)−C(5)−C(8)	125.22(14)	C(5)−C(8)−C(9)	133.44(14)
O(1)−C(1)−C(2)	133.13(16)	O(2)−C(3)−C(2)	125.03(16)	O(5)−C(6)−C(5)	111.89(13)	N(1)−C(9)−C(8)	123.17(14)
O(6)−C(1)−C(2)	107.37(13)	O(3)−C(3)−C(2)	111.45(13)				

Scheme 5. Resonance Structures of Compounds 21

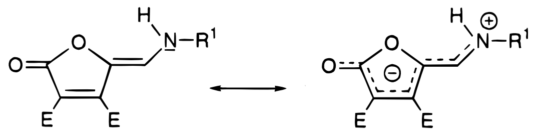

carbon atoms (bridgehead carbon) in **10** and **16**, observed at ca. 113 ppm, are shifted approximately 50 ppm to lower frequency compared to those of the free ligand, as a result of the change of hybridization from sp^2 to sp^3. These resonances are shifted ca. 20 ppm to higher frequency compared to those in complexes **4** (cf. Scheme 1; X = O), which is due to the change in the nature of the substituent R^3: i.e., a methyl or phenyl substituent in **4** versus an O-alkyl substituent in the present case. The former alkyne carbon atoms in complexes **10** and the ester-substituted alkene carbons in **16** resonate between 64.9 and 68.9 ppm, within the range generally observed for coordinated alkene carbon atoms.[63,66,67] The proton-bearing alkene carbons in **16** are shifted ca. 20 ppm to lower frequency (46.6 ppm) compared to the methyl ester substituted alkene carbons in **16**, which was also observed for **4**. The close resemblance of the ^1H and ^{13}C NMR data of complexes **16** and **4** points to the formation of the same regioisomer: i.e., initial bonding of the proton-substituted alkyne carbon in **8** to iron (cf. Scheme 3). This is in agreement with the formation of **20**, in which the proton-bearing carbon atoms of MP are C−C connected.

Complexes 11a,f. The ^1H and ^{13}C NMR data of **11a**,**f** are in agreement with the solid-state structure of **11a**. The sp^2-metalated carbon resonances, observed at ca. 189 ppm, compare well with those of the closely related complexes $Fe_2(CO)_5$(OIB), $Fe_2(CO)_5$(OPP) (cf. Chart 1), and **25** (cf. Scheme 8). The resonances of the π-coordinated alkene carbon are observed at ca. 77 ppm, close to the resonance of the corresponding carbon (78.4 ppm) in $Fe_2(CO)_5$[OPP(H)]. In comparison to the other $Fe_2(CO)_5$(OPP) complexes, $Fe_2(CO)_5$(OIB), and **25**, this carbon atom is shifted ca. 20 ppm to lower frequency due to the opposite σ, π coordination of the alkene in the latter complexes. An intact N═C(H) fragment is indicated by the imine proton resonances at ca. 8.1 ppm and the imine carbon resonances at ca. 177 ppm. The other signals are observed at the expected positions.

Complexes 13a,c. The ^1H and ^{13}C NMR data of complexes **13** are in agreement with the solid-state structure of **13c**. The new N−H protons give rise to broad doublets at 2.37 and 2.63 ppm, respectively, comparable with the resonances (2.57−2.82 ppm) observed for the N−H protons in the isostructural Ru_2CO_6[RCC(H)C(H)N(H)R].[61] The large ^3J coupling of the N−H proton with one of the methylene NCH_2 protons (^3J = 9.9 Hz) in **13a** and the somewhat smaller coupling with the *i*-PrC−H proton (^3J = 6.3 Hz) in **13c** indicate that these bonds are almost coplanar (Karplus−Conroy relation). This is consistent with the dihedral angle of 156.2(9)° between the N−H and the *i*-Pr C−H bond found in the solid-state structure of **13c**. The three methyl ester substituents on the allylic fragment are observed as three separate singlets between 3.72 and 3.92 ppm. The carbon resonances of the allylic fragment are found at about 158 ppm (μ_2), 99 ppm (central), and 70 ppm (terminal), comparable to the positions of the corresponding allylic carbon atoms in $Fe_2(CO)_6$[HCC(C(O)CH_3)C(O)CH_3)S-*t*-Bu][44] and Ru_2CO_6[RCC(H)C(H)N(H)R].[61] The shift of approximately 90 ppm of the μ_2 allylic carbon to higher frequency compared to the other is attributed to its σ,π-allyl bridging coordination mode.

The six terminal CO ligands of both **13a** and **13c** show temperature-dependent behavior, namely local scrambling of the carbonyls on one of the metal centers. Variable-temperature ^{13}C NMR spectra of **13c** in $CDCl_3$ show six separate signals at 203 K (216.5, 211.1, 208.8, 208.5, 207.9, and 206.4 ppm). At 263 K three signals of equal intensity at 211.4, 208.6, and 207.9 ppm are observed, and at 313 K, a fourth signal (210.6 ppm) of approximately 3 times the intensity of the other three has appeared. Individual assignment of the two $Fe(CO)_3$ moieties is not clear from this dynamic behavior but can reasonably be deduced from the presence of the low-frequency CO resonance at 216.5 ppm. This resonance is assigned to the carbonyl *trans* to the good σ(N) donor function. Consequently, the resonances at 216.5, 208.5, and 206.4 ppm correspond to the σ(N):σ(C)-coordinated $Fe^1(CO)_3$ moiety and the other resonances to the $Fe^2(CO)_3$ moiety, coordinated to the allylic system (cf. Scheme 2b).

Complexes 15f,g. The ^1H and ^{13}C NMR data of complexes **15** are in agreement with the solid-state structure of **15h**. The former imine proton resonances in complexes **15** are observed at ca. 5 ppm and those of the imine carbon atoms at ca. 63 ppm. These resonances are shifted approximately 3 and 100 ppm, respectively, to lower frequency compared to those of the free ligand as a result of the rehybridization from sp^2 to sp^3. The intact noncoordinating C(O)R^3 (R^3 = OMe, OEt, O-*i*-Pr) resonances are observed between 176.3 and 170.1 ppm: i.e., normal ester carbonyl resonances. The resonances of the coordinated alkene carbon atoms (63.9−68.1 ppm) are found at the same position as those in complexes **4** and **10**. The four terminal CO ligands are

---

[66] Mann, B. E.; Taylor, B. F. *^{13}C NMR Data of Organometallic Compounds*; Academic Press: London, 1981.

[67] Marks, T. J. *The Organic Chemistry of Iron*; Academic Press: New York, 1987.

Table 11. IR Data,[a] Elemental Analyses, and FD-Mass Data[b] of 10, 11, 13, 15, 16, and 19−23

compd	IR ν(CO) and ν(NH) (cm^{-1})	elem anal. obsd (calcd) (%) C	H	N	M
10a	2072 (s), 2013 (sh), 1994 (s), 1755 (m), 1734 (m), 1699 (m)	43.89 (43.75)	3.96 (3.90)	3.26 (3.19)	439 (439)
10b	2073 (s), 2014 (sh), 1997 (s), 1755 (m), 1733 (m), 1702 (m)	46.38 (46.27)	4.49 (4.53)	3.10 (3.00)	476 (476)
10c	2088 (s), 2008 (sh), 1993 (s), 1757 (m), 1735 (m), 1703 (m)	43.85 (43.76)	4.04 (3.90)	3.24 (3.19)	
10d	2075 (s), 2015 (sh), 1995 (s), 1759 (m), 1735 (m), 1704 (m)	45.11 (45.05)	4.28 (4.25)	3.07 (3.09)	
10e	2070 (s), 2010 (sh), 1993 (s), 1760 (m), 1735 (m), 1708 (m)	46.22 (46.27)	4.57 (4.53)	3.08 (3.00)	
10f	2070 (s), 2010 (sh), 1991 (s), 1757 (m), 1730 (m), 1708 (m)	44.88 (45.05)	4.29 94.23)	3.13 (3.09)	453 (453)
10g	2070 (s), 2010 (sh), 1990 (s), 1757 (m), 1736 (m), 1705 (m)	46.27 (46.27)	4.56 (4.53)	3.06 (3.00)	
10h	2065 (s), 2005 (sh), 1989 (s), 1760 (m), 1735 (m), 1703 (m)	not anal.			481 (481)
10i	2070 (s), 2005 (sh), 1990 (s), 1761 (m), 1735 (m), 1705 (m)	46.35 (46.27)	4.58 (4.53)	3.03 (3.00)	
10j	2065 (s), 2005 (sh), 1990 (s), 1759 (m), 1735 (m), 1705 (m)	47.36 (47.42)	4.93 (4.82)	2.93 (2.91)	
11a	2075 (s), 2012 (vs), 1988 (sh), 1956 (m), 1734 (m), 1703 (m)		not anal.		523 (523)
11f	2077 (s), 2013 (vs), 1990 (sh), 1959 (m), 1735 (m), 1705 (m)		not anal.		537 (537)
13a	3266 (w, NH), 2077 (s), 2038 (vs), 2007 (s), 1998 (s), 1730 (m), 1706 (m)	39.36 (39.24)	3.29 (3.11)	2.62 (2.54)	
13c	3259 (w, NH), 2076 (s), 2036 (vs), 2006 (s), 1997 (s), 1733 (m), 1705 (m)	39.22 (39.24)	3.06 (3.11)	2.61 (2.54)	
15f	2112 (s), 2045 (vs), 2016 (vs), 1744 (m), 1701 (b, m)	45.04 (44.93)	4.10 (3.98)	2.98 (2.91)	
15g	2113 (s), 2048 (vs), 2020 (vs), 1734 (m), 1699 (b, m)		not anal.		495 (495)
15h	2111 (s), 2047 (vs), 2018 (vs), 1733 (m), 1699 (b, m)	47.26 (47.17)	4.63 (4.56)	2.79 (2.75)	
16f	2063 (s), 1995 (sh), 1985 (s), 1754 (m), 1703 (w)	45.50 (45.59)	4.39 (4.34)	3.58 (3.54)	
16i	2060 (s), 1995 (sh), 1985 (s), 1749 (m), 1708 (w)	46.86 (46.97)	4.72 (4.68)	3.48 (3.42)	
19c	2085 (s), 2030 (sh), 2020 (s), 1795 (m), 1735 (m), 1695 (m)		not anal.		523 (523)
19f	2085 (s), 2033 (sh), 2018 (s), 1800 (m), 1737 (m), 1695 (m)	46.81 (46.95)	4.27 (4.32)	2.63 (2.61)	
19i	2083 (s), 2030 (sh), 2012 (s), 1796 (m), 1735 (m), 1710 (m)	48.10 (47.93)	4.68 (4.57)	2.50 (2.54)	
20c	2075 (s), 2020 (sh), 2010 (s), 1780 (m), 1690 (m)		not anal.		465 (465)
20f	2080 (s), 2026 (sh), 2010 (s), 1780 (m), 1695 (m)	47.57 (47.61)	4.50 (4.42)	2.96 (2.92)	
20i	2080 (s), 2020 (sh), 2010 (s), 1780 (m), 1693 (m)	48.60 (48.70)	4.75 (4.70)	2.89 (2.84)	
21c	3368 (w), 1740 (b, s), 1708 (sh), 1652 (s)	55.36 (53.52)	5.75 (5.62)	5.15 (5.20)	
21f	3364 (w), 1736 (b, s), 1698 (sh), 1649 (s)	55.04 (55.11)	6.11 (6.05)	4.95 (4.94)	
21i	3363 (w), 1738 (b, s), 1712 (sh), 1647 (s)		not anal.		
22c	1796 (s), 1746 (s), 1721 (sh), 1673 (w)				
22d	1797 (s), 1747 (s), 1719 (sh), 1675 (w)				
22f	1799 (s), 1748 (s), 1721 (sh), 1676 (w)				313 (314)
22g	1798 (s), 1748 (s), 1721 (sh), 1675 (w)				327 (328)
22h	1796 (s), 1749 (s), 1718 (sh), 1675 (w)				341 (342)
22i	1799 (s), 1748 (s), 1721 (sh), 1675 (w)				327 (328)
22j	1797 (s), 1747 (s), 1720 (sh), 1675 (w)				341 (342)
23c	1744 (s), 1705 (sh), 1654 (m), 1601 (m)				283 (283)
23f	1744 (s), 1707 (sh), 1657 (m), 1600 (m)				297 (297)
23i	1744 (s), 1712 (sh), 1657 (m), 1599 (m)				311 (311)

[a] Abbreviations: vs = very strong, s = strong, m = medium, w = weak, b = broad. Measured in CH_2Cl_2. [b] Observed (calculated) FD masses of molecular ion M^+ (*m*/*e*); the *M* values of the organometallic complexes are based upon the ^{56}Fe isotope.

Chart 1. Coordination Geometry of $Fe_2(CO)_5(OIB)$ and $Fe_2(CO)_5(OPP)$

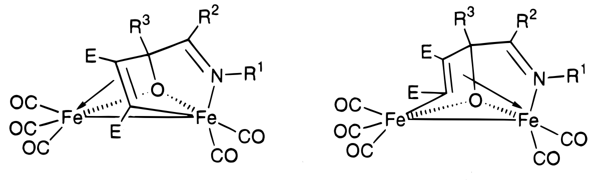

R^1= alkyl, R^2= H, R^3= O-alkyl (**11**)
R^1–R^2= $(CH)_4$, R^3= H

R^1= ^tAm, ^pTol, R^2= H, Ph R^3= Me, Ph
R^1–R^2= $(CH)_4$, R^3= Me, Ph

observed as four separate resonances between 206.1 and 201.6 ppm, which falls within the range normally observed for $Fe(CO)_4(\eta^2\text{-alkene})$ carbonyl resonances.[63,67]

Complexes 19 and 20. The NMR data of complexes **19** and **20** are in agreement with the structures in the solid state. The ^1H and ^{13}C NMR data closely resemble those of the isostructural complexes **6** (cf. Scheme 1).[9] The imine proton resonances of **19** and **20** are observed at ppm values (7.71−7.86 ppm) similar to those of complexes **6** and **10**. The protons of the former alkyne MP in **19** are observed as singlets at 6.70−6.82 ppm: i.e., normal positions for alkene protons. The two former MP protons in complexes **20** give rise to two doublets at ca. 6.9 and 4.7 ppm, which show relatively small coupling constants (^3J = 2.9−3.2 Hz). These resonances are shifted slightly (0.3 ppm) to lower frequency compared to those in **6**, and the coupling constants are very similar (3.3 Hz). On the basis of these similarities we propose the same linkage isomers for **20** as for **6**: i.e., with the two unsubstituted carbon atoms of the MP and the butenolide double bond C−C connected. This is further corroborated by the resonances of the two metalated carbon atoms and the carbon atoms involved in the C−C coupling reaction, which are observed at almost the same position as those in complexes **6**.

In complexes **19**, the FeC−***C***(sp^3) resonances are shifted ca. 13 ppm to higher frequency (76 ppm) compared to those in **20** as a result of substitution of the proton for a methyl ester group. As expected, the Fe***C***−C(sp^3) carbon resonances are observed at positions (68 ppm) almost identical with those in **20**. The other ^{13}C resonances of the carbons in the heterocyclic ligand, which are not involved in the C−C coupling reaction, are found at positions identical with those in $Fe(CO)_3$-(butenolide) (**10**).

Compounds 21. The NMR data in solution are in agreement with the structure in the solid state. The new N−H proton resonance in **21c** is observed at 7.74 ppm as a broad double doublet due to coupling with the exocyclic alkene proton and the *i*-Pr C−H proton. In **21f**,**i**, the N−H proton resonances are observed as broad doublets at 7.76 and 7.29 ppm due to the coupling with the exocyclic alkene proton. The large coupling (^3J = 10.7−14.0 Hz) between the N−H proton and the exocyclic alkene proton in **21** suggests that the N−H and C−H bonds are almost coplanar. This is in agreement

Table 12. ^{1}H NMR Data[a] of 10, 11, 13, 15, 16, and 19−23

compd	δ
10a	7.76 (1H, s, N=C*H*), 3.83, 3.72 (2 × 3H, s, 2 × $\mathrm{C(O)OC}H_3$), 3.48 (3H, s, $\mathrm{OC}H_3$), 3.42 (2H, t, 7.3 Hz, $\mathrm{NC}H_2$), 1.60 (2H, m, $\mathrm{NCH_2C}H_2$), 0.83 (3H, t, 7.3 Hz, $\mathrm{CH_2C}H_3$)
10b	7.76 (1H, b d, 1.1 Hz, N=C*H*), 3.85, 3.77 (2 × 3H, s, 2 × $\mathrm{C(O)OC}H_3$), 3.50 (3H, s, $\mathrm{OC}H_3$), 3.40 (1H, d, 11.6 Hz, NC*H*H), 3.30 (1H, dd, 11.6 Hz, 1.1 Hz, NCH*H*), 0.85 (9H, t, 7.3 Hz, $\mathrm{CH_2(C}H_3)_3$)
10c	7.82 (1H, s, N=C*H*), 3.83, 3.75 (2 × 3H, s, 2 × $\mathrm{C(O)OC}H_3$), 3.77 (1H, sept, 6.5 Hz, *i*-Pr C*H*), 3.49 (3H, s, $\mathrm{OC}H_3$), 1.29, 1.09 (2 × 3H, d, 6.5 Hz, 2 × *i*-Pr $\mathrm{C}H_3$)
10d	7.83 (1H, s, N=C*H*), 3.90, 3.71 (2 × 1H, dq, 7.0 Hz, 9.4 Hz, 2 × OCH*H*), 3.84, 3.78 (2 × 3H, s, 2 × $\mathrm{C(O)OC}H_3$), 3.78 (1H, sept, 6.6 Hz, *i*-Pr C*H*), 1.30 (3H, t, 7.0 Hz, $\mathrm{OCH_2C}H_3$), 1.30, 1.07 (2 × 3H, d, 6.6 Hz, 2 × *i*-Pr $\mathrm{C}H_3$)
10e	7.84 (1H, s, N=C*H*), 4.20 (1H, sept, 6.1 Hz, O-*i*-Pr C*H*), 3.88, 3.76 (2 × 3H, s, 2 × $\mathrm{C(O)OC}H_3$), 3.80 (1H, sept, 6.5 Hz, N-*i*-Pr C*H*), 1,34, 1.30 (2 × 3H, d, 6.1 Hz, 2 × O-*i*-Pr $\mathrm{C}H_3$), 1.28, 1.09 (2 × 3H, d, 6.5 Hz, 2 × N-*i*-Pr $\mathrm{C}H_3$)
10f	7.83 (1H, s, N=C*H*), 3.86, 3.77 (2 × 3H, s, 2 × $\mathrm{C(O)OC}H_3$), 3.53 (3H, s, $\mathrm{OC}H_3$), 1.34 (9H, s, $\mathrm{C(C}H_3)_3$)
10g	7.54 (1H, s, N=C*H*), 3.89, 3.71 (2 × 1H, dq, 7.0 Hz, 9.5 Hz, 2 × OCH*H*), 3.86, 3.78 (2 × 3H, s, 2 × $\mathrm{C(O)OC}H_3$), 1.33 (9H, s, $\mathrm{C(C}H_3)_3$), 1.31 (3H, t, 7.0 Hz, $\mathrm{OCH_2C}H_3$)
10h	7.80 (1H, s, N=C*H*), 4.19 (1H, sept, 6.0 Hz, O-*i*-Pr C*H*), 3.82, 3.74 (2 × 3H, s, 2 × $\mathrm{C(O)OC}H_3$), 1.32, 1.26 (2 × 3H, d, 6.1 Hz, 2 × O-*i*-Pr $\mathrm{C}H_3$), 1.30 (9H, s, $\mathrm{C(C}H_3)_3$)
10i	7.60 (1H, s, N=C*H*), 3.85, 3.78 (2 × 3H, s, 2 × $\mathrm{C(O)OC}H_3$), 3.52 (3H, s, $\mathrm{OC}H_3$), 1.51, 1.50 (2 × 1H, dq, 4.6 Hz, 7.5 Hz, 2 × CH*H*), 1.48, 1.28 (2 × 3H, s, 2 × $\mathrm{CC}H_3$), 0.60 (3H, t, 7.5 Hz, $\mathrm{CH_2C}H_3$)
10j	7.79 (1H, s, N=C*H*), 3.89, 3.72 (2 × 1H, dq, 7.0 Hz, 9.8 Hz, 2 × OCH*H*), 3.86, 3.78 (2 × 3H, s, 2 × $\mathrm{C(O)OC}H_3$), 1.53, 1.51 (2 × 1H, dq, 6.3 Hz, 7.5 Hz, 2 × CCH*H*), 1.51, 1.34 (2 × 3H, s, 2 × $\mathrm{CC}H_3$), 1.31 (3H, t, 7.0 Hz, $\mathrm{OCH_2C}H_3$), 0.70 (3H, t, 7.5 Hz, $\mathrm{CH_2C}H_3$)
11a	8.12 (1H, s, N=C*H*), 3.80, 3.77, 3.23 3 × 3H, s, 3 × $\mathrm{OC}H_3$), 3.41 (2H, m, $\mathrm{NC}H_2$), 1.81 (2H, m, $\mathrm{NCH_2C}H_2$), 0.89 (3H, t, 7.4 Hz, $\mathrm{CH_2C}H_3$)
11f	8.06 (1H, s, N=C*H*), 3.82, 3.75 (2 × 3H, s, 2 × $\mathrm{C(O)OC}H_3$), 3.25 (3H, s, $\mathrm{OC}H_3$), 1.37 (9H, s, $\mathrm{C(C}H_3)_3$)
13a	3.92, 3.88, 3.75 (3 × 3H, s, 3 × $\mathrm{OC}H_3$), 2.49 (1H, m, 9.9 Hz, NCH*H*), 2.37 (1H, br d, 9.6 Hz, N*H*), 1.60 (1H, m, 9.6 Hz, 9.9 Hz, NC*H*H), 1.38, 1.26 (2 × 1H, m, 2 × $\mathrm{NCH_2C}H$), 0.83 (3H, t, 7.4 Hz, $\mathrm{CH_2C}H_3$)
13c	3.90, 3.87, 3.72 (3 × 3H, s, 3 × $\mathrm{C(O)OC}H_3$), 2.63 (1H, br d, 6.3 Hz, N*H*), 2.45 (1H, dsept, 6.3 Hz, 6.4 Hz, *i*-Pr−C*H*), 0.97, 0.94 (2 × 3H, d, 6.4 Hz, 2 × *i*-Pr $\mathrm{C}H_3$)
15f	5.01 (1H, s, C*H*), 3.86, 3.80, 3.79 (3 × 3H, s, 3 × $\mathrm{C(O)OC}H_3$), 1.35 (9H, s, $\mathrm{C(C}H_3)_3$)
15g	4.98 (1H, s, C*H*), 4.37, 4.26 (2 × 1H, dq, 10.9 Hz, 7.1 Hz, 2 × OC*H*H), 3.80, 3.79 (2 × 3H, s, 2×$\mathrm{OC}H_3$), 1.36 (3H, t, 7.1 Hz, $\mathrm{CH_2C}H_3$), 1.35 (9H, s, $\mathrm{C(C}H_3)_3$)
15h	5. 13 (1H, sept, 6.3 Hz, *i*-Pr−C*H*), 4.92 (1H, s, C*H*), 3.80, 3.79 (2 × 3H, s, 2 × $\mathrm{OC}H_3$), 1.36 (9H, s, $\mathrm{C(C}H_3)_3$), 1.36, 1.32 (2 × 3H, d, 6.3 Hz, 2 × *i*-Pr $\mathrm{C}H_3$)
16f	7.82 (1H, s, N=C*H*), 4.05 (1H, s, C=C*H*), 3.74 (3H, s, $\mathrm{C(O)OC}H_3$), 3.42 (3H, s, $\mathrm{OC}H_3$), 1.31 (9H, s, $\mathrm{C(C}H_3)_3$)
16i	7.79 (1H, s, N=C*H*), 4.08 (1H, s, C=C*H*), 3.78 (3H, s, $\mathrm{C(O)OC}H_3$), 3.46 (3H, s, $\mathrm{OC}H_3$), 1.59, 1.48 (2 × 1H, dq, 7.4 Hz, 15 Hz, 2 × CCH*H*), 1.47, 1.29 (2 × 3H, s, 2 × $\mathrm{CC}H_3$), 0.67 (3H, t, 7.5 Hz, $\mathrm{CH_2C}H_3$)
19c	7.86 (1H, s, N=C*H*), 6.70 (1H, s, C=C*H*), 4.09 (1H, sept, 6.5 Hz, *i*-Pr C*H*), 3.73, 3.72, 3.66 (3 × 3H, s, 3 × $\mathrm{C(O)OC}H_3$), 3.57 (3H, s, $\mathrm{OC}H_3$), 1.34, 1.25 (2 × 3H, d, 6.5 Hz, 2 × *i*-Pr $\mathrm{C}H_3$)
19f	7.83 (1H, s, N=C*H*), 6.80 (1H, s, C=C*H*), 3.73, 3.70, 3.67 (3 × 3H, s, 3 × $\mathrm{C(O)OC}H_3$), 3.58 (3H, s, $\mathrm{OC}H_3$), 1.35, (9H, s, $\mathrm{C(C}H_3)_3$)
19i	7.76 (1H, s, N=C*H*), 6.82 (1H, s, C=C*H*), 3.72, 3.70, 3.66 (3 × 3H, s, 3 × $\mathrm{C(O)OC}H_3$), 3.59 (3H, s, $\mathrm{OC}H_3$), 1.77, 1.68 (2 × 1H, dq, 7.4 Hz, 14.3 Hz, 2 × CCH*H*), 1.28, 1.22 (2 × 3H, s, 2 × $\mathrm{CC}H_3$), 0.78 (3H, t, 7.4 Hz, $\mathrm{CH_2C}H_3$)
20c	7.82 (1H, s, N=C*H*), 6.82 (1H, d, 2.9 Hz, C=C*H*), 4.64 (1H, d, 2.9 Hz, C*H*), 4.04 (1H, sept, 6.5 Hz, *i*-Pr C*H*), 3.78, 3.72 (2 × 3H, s, 2 × $\mathrm{C(O)OC}H_3$), 3.58 (3H, s, $\mathrm{OC}H_3$), 1.32, 1.24 (2 × 3H, d, 6.5 Hz, 2 × *i*-Pr $\mathrm{C}H_3$)
20f	7.77 (1H, s, N=C*H*), 6.93 (1H, d, 3.2 Hz, C=C*H*), 4.73 (1H, d, 3.2 Hz, C*H*), 3.78, 3.71 (2 × 3H, s, 2 × $\mathrm{C(O)OC}H_3$), 3.55 (3H, s, $\mathrm{OC}H_3$), 1.36 (9H, s, $\mathrm{C(C}H_3)_3$)
20i	7.71 (1H, s, N=C*H*), 6.95 (1H, d, 3.2 Hz, C=C*H*), 4.71 (1H, d, 3.2 Hz, C*H*), 3.76, 3.70 (2 × 3H, s, 2 × $\mathrm{C(O)OC}H_3$), 3.55 (3H, s, $\mathrm{OC}H_3$), 1.77, 1.69 (2 × 1H, dq, 7.4 Hz, 14.8 Hz, 2 × CCH*H*), 1.30, 1.23 (2 × 3H, s, 2 × $\mathrm{CC}H_3$), 0.78 (3H, t, 7.4 Hz, $\mathrm{CH_2C}H_3$)
21c	7.74 (1H, br dd, 14.0 Hz, 7,5 Hz, N*H*), 6.95 (1H, d, 14.0 Hz, NC*H*), 3.95, 3.81 (2 × 3H, s, 2 × $\mathrm{C(O)OC}H_3$), 3.70 (1H, dsept, 6.5 Hz, 7.5 Hz, *i*-Pr C*H*), 1.36 (6H, d, 6.5 Hz, 2 × *i*-Pr $\mathrm{C}H_3$)
21f	7.76 (1H, br d, 10.7 Hz, N*H*), 6.98 (1H, d, 10.7 Hz, NC*H*), 3.95, 3.80 (2 × 3H, s, 2 × $\mathrm{C(O)OC}H_3$), 1.41 (9H, s, $\mathrm{C(C}H_3)_3$)
21i	7.29 (1H, br d, 14.0 Hz, N*H*), 6.98 (1H, d, 14.0 Hz, NC*H*), 3.95, 3.81 (2 × 3H, s, 2 × $\mathrm{C(O)OC}H_3$), 1.65 (2H, q, 7.4 Hz, $\mathrm{NCC}H_2$), 1.34 (6H, s, 2 × $\mathrm{CC}H_3$), 0.90 (3H, t, 7.4 Hz, $\mathrm{CH_2C}H_3$)
22c	7.67 (1H, s, N=C*H*), 3.93, 3.86 (2 × 3H, s, 2 × $\mathrm{C(O)OC}H_3$), 3.43 (3H, s, $\mathrm{OC}H_3$), 3.47 (1H, sept, 6.3 Hz, *i*-Pr C*H*), 1.12 (6H, d, 6.3 Hz, 2 × *i*-Pr $\mathrm{C}H_3$)
22d	7.68 (1H, s, N=C*H*), 3.88, 3.82 (2 × 3H, s, 2 × $\mathrm{C(O)OC}H_3$), 3.69 (2H, q, 7.0 Hz, $\mathrm{OCH_2}$), 3.43 (1H, sept, 6.3 Hz, *i*-Pr C*H*), 1.24 (3H, t, 7.0 Hz, $\mathrm{OCH_2C}H_3$), 1.07 (6H, d, 6.3 Hz, 2 × *i*-Pr $\mathrm{C}H_3$)
22f	7.60 (1H, s, N=C*H*), 3.92, 3.85 (2 × 3H, s, 2 × $\mathrm{C(O)OC}H_3$), 3.43 (3H, s, $\mathrm{OC}H_3$), 1.14 (9H, s, $\mathrm{C(C}H_3)_3$)
22g	7.63 (1H, s, N=C*H*), 3.93, 3.85 (2 × 3H, s, 2 × $\mathrm{C(O)OC}H_3$), 3.69, 3.61 (2 × 1H, dq, 7.1 Hz, 10.1 Hz, 2 × OCH*H*), 1.28 (3H, t, 7.1 Hz, $\mathrm{OCH_2C}H_3$), 1.14 (9H, s, $\mathrm{C(C}H_3)_3$)
22i	7.55 (1H, s, N=C*H*), 3.89, 3.81 (2 × 3H, s, 2 × $\mathrm{C(O)OC}H_3$), 3.40 (3H, s, $\mathrm{OC}H_3$), 1.42 (2H, q, 7.5 Hz $\mathrm{C}H_2\mathrm{CH_3}$), 1.05 (6H, s, 2 × $\mathrm{C(C}H_3)$, 0.69 (3H, t, 7.4 Hz, $\mathrm{CH_2C}H_3$)
22j	7.56 (1H, s, N=C*H*), 3.83, 3.77 (2 × 3H, s, 2 × $\mathrm{C(O)OC}H_3$), 3.69, 3.61 (2 × 1H, dq, 7.0 Hz, 10.1 Hz, 2 × OCH*H*), 1.38 (2H, q, 7.4 Hz, $\mathrm{C}H_2\mathrm{CH_3}$), 1.20 (3H, t, 7.0 Hz, $\mathrm{OCH_2C}H_3$), 1.01 (6H, s, 2 × $\mathrm{C(C}H_3)$, 0.65 (3H, t, 7.6 Hz, $\mathrm{CH_2C}H_3$)
23c	7.07 (1H, s, N=C*H*), 5.31 (1H, sept, 6.8 Hz, *i*-Pr C*H*), 3.91, 3.88 (2 × 3H, s, 2 × $\mathrm{C(O)OC}H_3$), 3.76 (3H, s, $\mathrm{OC}H_3$), 1.36 (6H, d, 6.8 Hz, 2 × *i*-Pr $\mathrm{C}H_3$)
23d	7.12 (1H, s, N=C*H*), 5.32 (1H, sept, 6.8 Hz, *i*-Pr C*H*), 3.92 (2H, q, 7.0 Hz, $\mathrm{OC}H_2$), 3.91, 3.89 (2 × 3H, s, 2 × $\mathrm{C(O)OC}H_3$), 1.35 (6H, d, 6.8 Hz, 2 × *i*-Pr $\mathrm{C}H_3$), 1.35 (3H, t, 7.0 Hz, $\mathrm{OCH_2C}H_3$)
23e	7.17 (1H, s, N=C*H*), 5.31 (1H, sept, 6.8 Hz, O-*i*-Pr C*H*), 4.16 (1H, sept, 6.1 Hz, *i*-Pr C*H*), 3.91, 3.89 (2 × 3H, s, 2 × $\mathrm{C(O)OC}H_3$), 1.35 (6H, d, 6.8 Hz, 2 × *i*-Pr $\mathrm{C}H_3$), 1.17 (6H, d, 6.1 Hz, 2 × *i*-Pr $\mathrm{C}H_3$)

[a] δ values, in ppm relative to TMS, measured in $\mathrm{CDCl_3}$ at 293 K and 300.13 MHz. Abbreviations: s = singlet, d = doublet, t = triplet, q = quartet, sept = septet, dq = double quartet, dsept = double septet.

with the dihedral angle of 175.1(15)° observed in the solid-state structure of **21c**. Likewise, the additional coupling of the N−H proton with the *i*-Pr CH proton in **21c** is relatively large ($^3J = 7.5$ Hz), which is consistent with the dihedral angle of 172.9(15)° between these bonds in **21c**. The exocyclic alkene proton resonances are observed around 6.9 ppm, a relatively high position for an alkene proton, which is probably due to the partial imine character of the C−N bond (cf. Scheme 5). The alkene carbon atoms, observed between 101 and 128 ppm, are shifted approximately 40−60 ppm to higher frequency compared to those in **10** due to the liberation from the metal. The resonances of the inserted CO and the carboxyl ester carbons (166−163 ppm) are shifted somewhat to lower frequency.

Spectroscopic Characterization and Assignment of Compounds 22 and 23. The structures of compounds **22** and **23** shown in Scheme 4 are assigned on the basis of their IR, FD-mass, ^{1}H and ^{13}C NMR spectroscopic properties.

Table 13. ^{13}C NMR Data[a] of 10, 11, 13, 16, 16, and 19−23

compd	δ
10a	208.8, 207.6, 205.1 (*C*O), 178.4 (*C*=N), 170.9, 170.0, 168.6 (2 × ester *C*O, ring *C*O), 113.1 (N=C*C*), 67.0 (N*C*H$_2$), 68.0, 65.4(2 × C=*C*), 54.4, 52.7, 52.4 (3 × OCH$_3$), 23.1 (NCH$_2$*C*H$_2$), 11.5 (CH$_2$*C*H$_3$)
10b	208.6, 207.5, 205.1 (*C*O), 183.6 (*C*=N), 171.0, 169.9, 168.5 (2 × ester *C*O, ring *C*O), 113.0 (N=C*C*), 75.0 (N*C*H$_2$), 68.3, 65.6 (2 × C=*C*), 54.5, 52.7, 52.3 (3×OCH$_3$), 34.5 (*C*(CH$_3$)$_3$), 28.5 (C(*C*H$_3$)$_3$)
10c	208.9, 207.8, 205.1 (*C*O), 176.0 (*C*=N), 170.8, 169.9, 168.8 (2 × ester *C*O, ring *C*O), 113.3 (N=C*C*), 67.3, 66.5 (2 × C=*C*), 65.1 (*i*-Pr *C*H), 54.4, 52.6, 52.4 (3×OCH$_3$), 23.7, 22.2 (*i*-Pr *C*H$_3$)
10d	209.0, 207.8, 205.2 (*C*O), 176.2 (*C*=N), 170.9, 170.0, 168.6 (2 × ester *C*O, ring *C*O), 113.1 (N=C*C*), 67.7, 65.6 (2 × C=*C*), 65.1 (*i*-Pr *C*H), 61.2 (O*C*H$_2$), 54.5, 52.6 (2 × OCH$_3$), 23.7, 22.2 (*i*-Pr *C*H$_3$), 15.4 (OCH$_2$*C*H$_3$)
10e	209.0, 207.8, 205.3 (*C*O), 176.7 (*C*=N), 170.6, 169.8, 168.7 (2 × ester *C*O, ring *C*O), 113.6 (N=C*C*), 71.2 (O-*i*-Pr *C*H), 68.9, 66.6 (2 × C=*C*), 65.1 (N-*i*-Pr *C*H), 54.5, 52.5 (2 × OCH$_3$), 25.7, 23.7, 23.6, 22.2 (4 × *i*-Pr *C*H$_3$)
10f	209.4, 208.5, 205.5 (*C*O), 176.3 (*C*=N), 170.3, 169.8, 168.6 (2 × ester *C*O, ring *C*O), 113.3 (N=C*C*), 66.1, 65.0 (2 × C=*C*), 65.8 (*C*(CH$_3$)$_3$), 54.2, 52.7, 52.3 (3 × OCH$_3$), 30.9 (C(*C*H$_3$)$_3$)
10g	209.4, 208.5, 205.6 (*C*O), 176.5 (*C*=N), 170.8, 169.9, 168.6 (2 × ester *C*O, ring *C*O), 113.3 (N=C*C*), 66.6, 65.1 (2 × C=*C*), 65.8 (*C*(CH$_3$)$_3$), 61.1 (O*C*H$_2$), 54.5, 52.6 (2 × OCH$_3$), 30.9 (C(*C*H$_3$)$_3$), 15.4 (OCH$_2$*C*H$_3$)
10h	209.7, 208.6, 205.8 (*C*O), 177.2 (*C*=N), 170.3, 169.4, 168.6 (2 × ester *C*O, ring *C*O), 113.5 (N=C*C*), 70.9 (O-*i*-Pr *C*H), 68.2, 64.9 (2 × C=*C*), 65.8 (*C*(CH$_3$)$_3$), 54.2, 52.3 (2 × OCH$_3$), 31.0 (C(*C*H$_3$)$_3$), 25.2, 23.6 (2 × *i*-Pr *C*H$_3$)
10i	209.4, 208.4, 205.5 (*C*O), 177.4 (*C*=N), 170.7, 169.8, 168.5 (2 × ester *C*O, ring *C*O), 113.3 (N=C*C*), 68.3 (*C*(CH$_3$)$_2$), 66.6, 64.9 (2 × C=*C*), 54.4, 52.6, 52.2 (3 × OCH$_3$), 34.9, 30.9 (2 × C(*C*H$_3$), 26.7 (C*C*H$_2$), 8.3 (CH$_2$*C*H$_3$)
10j	209.4, 208.4, 205.6 (*C*O), 177.7 (*C*=N), 170.7, 169.8, 168.6 (2 × ester *C*O, ring *C*O), 113.1 (N=C*C*), 68.4 (*C*(CH$_3$)$_2$), 66.6, 64.9 (2 × C=*C*), 61.0 (O*C*H$_2$), 54.4, 52.6 (2 × OCH$_3$), 34.9, 31.0 (2 × C(*C*H$_3$), 26.7 (C*C*H$_2$), 15.4 (OCH$_2$*C*H$_3$), 8.4 (CH$_2$*C*H$_3$)
11a	211.4, 207.1 (*C*O), 189.4 (Fe−*C*=C), 176.2 (*C*=N), 172.6, 168.4 (2 × ester *C*O), 117.1 (O*C*O), 78.4 (F−C=*C*), 65.9 (N*C*H$_2$), 52.7, 52.4 (2 × OCH$_3$), 22.8 (NCH$_2$*C*H$_2$), 11.2 (CH$_2$*C*H$_3$)
11f	211.6, 206.9(*C*O), 188.6 (Fe−*C*=C), 177.3 (*C*=N), 171.3, 168.6 (2 × ester *C*O), 117.8 (O*C*O), 82.4 (Fe−C=*C*), 65.5 (*C*(CH$_3$)$_3$), 52.9, 52.3 (2 × OCH$_3$), 30.2 (C(*C*H$_3$)$_3$)
13a	211.3, 207.8, 207.7 (*C*O), 174.9, 170.7, 167.3 (3 × ester *C*O), 157.8 (NCC*C*), 99.5 (NC*C*), 70.2 (N*C*), 64.3 (N*C*H$_2$), 54.1, 53.6, 53.2 (3 × O*C*H$_3$), 21.0 (NCH$_2$*C*H$_2$), 11.2 (CH$_2$*C*H$_3$)
13c	211.4, 208.6, 207.9 (*C*O), 175.0, 170.8, 167.4 (3 × ester *C*O), 157.4 (NCC*C*), 99.4 (NC*C*), 68.9 (N*C*), 60.9 (*i*-Pr-*C*H), 54.1, 53.6, 53.0 (3 × O*C*H$_3$), 21.5, 19.5 (× *i*-Pr-*C*H$_3$)
15f	206.0, 204.6, 201.7, 201.6 (*C*O), 176.3, 174.5, 172.2, 170.1 (3 × ester *C*O, ring *C*O), 67.5, 64.3 (2 × C=*C*), 63.1 (ring *C*H), 57.4 (*C*(CH$_3$)$_3$), 54.2, 53.7, 53.7 (3 × OCH$_3$), 27.8 (C(*C*H$_3$)$_3$)
15g	206.2, 204.6, 201.8, 201.7 (*C*O), 176.3, 174.0, 172.2, 170.3 (3 × ester *C*O, ring *C*O), 68.0, 64.0 (2 × C=*C*), 63.3 (ring *C*H), 62.8 (O*C*H$_2$), 57.4 (*C*(CH$_3$)$_3$), 54.2, 53.7 (2 × OCH$_3$), 27.9 (C(*C*H$_3$)$_3$), 14.7 (OCH$_2$*C*H$_3$)
15h	206.1, 204.6, 201.7, 201.6 (*C*O), 176.3, 173.4, 172.0, 170.2 (3 × ester *C*O, ring *C*O), 70.4 (O-*i*-Pr *C*H), 68.1, 63.9 (2 × C=*C*), 63.3 (ring *C*H), 57.2 (*C*(CH$_3$)$_3$), 54.0, 53.5 (2 × O*C*H$_3$), 27.7 (C(*C*H$_3$)$_3$), 22.1, 21.9 (2 × *i*-Pr *C*H$_3$)
16f	209.6, 208.5, 207.9 (*C*O), 176.2 (*C*=N), 172.3, 171.2 (ester *C*O, ring *C*O), 112.3 (N=C*C*), 67.8 (HC=*C*), 65.7 (*C*(CH$_3$)$_3$), 52.5, 51.9 (2 × OCH$_3$), 46.6 (H*C*=C), 30.9 (C(*C*H$_3$)$_3$)
16i	209.6, 209.4, 207.9 (*C*O), 177.4 (*C*=N), 172.3, 171.2 (ester *C*O, ring *C*O), 112.4 (N=C*C*), 67.9 (HC=*C*), 67.8 (*C*(CH$_3$)$_2$), 52.5, 51.8 (2 × OCH$_3$), 46.6 (H*C*=C), 34.7, 31.4 (2 × C(*C*H$_3$), 26.7 (C*C*H$_2$), 8.3 (CH$_2$*C*H$_3$)
19c	207.9, 205.0, 204.7 (*C*O), 174.5, 173.6, 170.4, 169.7 (3 × ester *C*O, ring *C*O), 169.6 (*C*=N), 168.0 (Fe*C*=CH), 147.7 (FeC=*C*H), 115.1 (N=C*C*), 76.6 (FeC−*C*), 70.9 (FeC−C), 64.7 (*i*-Pr *C*H), 55.0, 53.5, 53.1, 52.7 (4 × OCH$_3$), 24.2, 22.7 (2 × *i*-Pr *C*H$_3$)
19f	208.0, 206.1, 204.6 (*C*O), 174.5, 173.6, 170.8, 169.5 (3 × ester *C*O, ring *C*O), 169.6 (*C*=N), 168.2 (Fe*C*=CH), 149.1 (FeC=*C*H), 114.5 (N=C*C*), 76.5 (FeC−*C*), 72.6 (Fe*C*-C), 66.0 (*C*(CH$_3$)$_3$), 55.0, 53.5, 53.1, 52.7 (4 × OCH$_3$), 30.0 (C(*C*H$_3$)$_3$)
19i	208.0, 205.7, 204.2 (*C*O), 174.3, 173.2, 170.8, 169.3 (3 × ester *C*O, ring *C*O), 170.6 (*C*=N), 168.0 (Fe*C*=CH), 149.0 (FeC=*C*H), 114.5 (N=C*C*), 76.3 (FeC−*C*), 72.5 (Fe*C*−C), 69.2 (*C*(CH$_3$)$_2$), 54.7, 53.3, 53.0, 52.5 (4 × OCH$_3$), 33.9, 27.8 (2 × C(*C*H$_3$), 26.3 (C*C*H$_2$), 8.7 (CH$_2$*C*H$_3$)
20c	209.9, 205.0, 204.3 (*C*O), 176.1, 174.0, 173.4, (2 × ester *C*O, ring *C*O), 169.8 (*C*=N), 162.8 (Fe*C*=C), 149.1 (FeC=*C*), 118.3 (N=C*C*), 68.0 (Fe*C*−C), 64.8 (*i*-Pr *C*H), 63.1 (FeC−*C*), 54.9, 53.4, 52.6 (3 × OCH$_3$), 23.9, 22.9 (2 × *i*-Pr *C*H$_3$)
20f	210.1, 206.1, 204.2 (*C*O), 176.2, 173.8, 173.6 (2 × ester *C*O, ring *C*O), 170.6 (*C*=N), 163.0 (Fe*C*=C), 150.2 (FeC=*C*), 117.7 (N=C*C*), 68.9 (Fe*C*−C), 66.8 (*C*(CH$_3$)$_3$), 62.8 (FeC−*C*), 54.6, 53.4, 52.6 (3 × OCH$_3$), 30.0 (C(*C*H$_3$)$_3$)
20i	210.2, 205.8, 204.0 (*C*O), 176.1, 173.7, 171.3 (2 × ester *C*O, ring *C*O), 170.6 (*C*=N), 163.0 (Fe*C*=C), 150.2 (FeC=*C*), 117.8 (N=C*C*), 68.9 (Fe*C*−C), 66.9 (*C*(CH$_3$)$_2$), 62.9 (FeC−*C*), 54.6, 53.3, 52.5 (3 × OCH$_3$), 34.0, 28.0 (2 × C*C*H$_3$), 26.6 (C*C*H$_2$), 8.7 (CH$_2$*C*H$_3$)
21c	166.2, 163.7, 163.2 (2 × ester *C*O, ring *C*O), 145.0 (HC=*C*), 134.7 (C=*C*H), 127.1, 101.5 (2 × ring C=*C*), 54.0, 53.3, 52.6 (2 × O*C*H$_3$, *i*-Pr *C*H), 23.7 (2 × *i*-Pr *C*H$_3$)
21f	166.1, 163.8, 163.3 (2 × ester *C*O, ring *C*O), 144.8 (HC=*C*), 132.4 (C=*C*H), 127.3, 101.3 (2 × ring C=*C*), 56.3 (*C*(CH$_3$)$_3$), 54.0, 52.5 (2 × O*C*H$_3$), 30.0 (C(*C*H$_3$)$_3$)
21i	165.9, 163.7, 163.2 (2 × ester *C*O, ring *C*O), 145.0 (HC=*C*), 132.4 (C=*C*H), 127.3, 101.8 (2 × ring C=*C*), 54.0, 52.6 (2 × O*C*H$_3$), 35.7 (2 × C*C*H$_3$), 27.3 (*C*H$_2$CH$_3$), 9.0 (CH$_2$*C*H$_3$)
22c	163.8, 160.5, 160.0 (2 × ester *C*O, ring *C*O), 154.1 (*C*=N), 153.4 (C=*C*), 130.9 (C=*C*), 106.3 (O*C*O), 60.7 (*i*-Pr *C*H), 53.5, 53.4, 52.2 (3 × OCH$_3$), 23.5 (2 × *i*-Pr *C*H$_3$)
22d	164.0, 160.7, 160.3 (2 × ester *C*O, ring *C*O), 154.7 (*C*=N), 153.7 (C=*C*), 132.0 (C=*C*), 106.5 (O*C*O), 61.2 (O*C*H$_2$), 60.8 (*i*-Pr *C*H), 53.6, 53.4 (2 × OCH$_3$), 23.6 (2 × *i*-Pr *C*H$_3$), 15.3 (OCH$_2$*C*H$_3$)
22f	164.1, 160.9, 160.3 (2 × ester *C*O, ring *C*O), 154.1 (C=*C*), 151.1 (*C*=N), 130.8 (C=*C*), 107.2 (O*C*O), 58.8 (*C*(CH$_3$)$_3$), 53.7, 53.5, 52.5 (3 × OCH$_3$), 29.3 (C(*C*H$_3$)$_3$)
22g	164.2, 160.9, 160.1 (2 × ester *C*O, ring *C*O), 154.2 (C=*C*), 152.0 (*C*=N), 130.8 (C=*C*), 107.2 (O*C*O), 61.3 (O*C*H$_2$), 58.6 (*C*(CH$_3$)$_3$), 53.6, 53.4 (2 × OCH$_3$), 29.4 (C(*C*H$_3$)$_3$), 15.4 (OCH$_2$*C*H$_3$)
22h	164.4, 160.9, 160.6 (2 × ester *C*O, ring *C*O), 153.7 (C=*C*), 152.5 (*C*=N), 131.4 (C=*C*), 107.5 (O*C*O), 70.4 (*i*-Pr *C*H), 58.6 (*C*(CH$_3$)$_3$), 53.7, 53.3 (2 × OCH$_3$), 29.3 (C(*C*H$_3$)$_3$), 24.7, 23.8 (*i*-Pr *C*H$_3$)
22i	164.2, 161.0, 160.4 (2 × ester *C*O, ring *C*O), 154.0 (C=*C*), 152.3 (*C*=N), 131.1 (C=*C*), 107.6 (O*C*O), 61.2 (*C*(CH$_3$)$_2$), 53.8, 53.6, 52.6 (3 × OCH$_3$), 35.8 (*C*H$_2$CH$_3$), 26.7, 26.2 (2 × C(*C*H$_3$), 8.8 (CH$_2$*C*H$_3$)
22j	164.1, 160.8, 160.4 (2 × ester *C*O, ring *C*O), 153.9 (C=*C*), 152.7 (*C*=N), 131.0 (C=*C*), 107.4 (O*C*O), 61.2 (O*C*H$_2$), 61.1 (*C*(CH$_3$)$_2$), 53.7, 53.3 (2 × OCH$_3$), 35.7 (*C*H$_2$CH$_3$), 26.5, 26.1 (2 × C(*C*H$_3$), 15.3 (OCH$_2$*C*H$_3$), 8.6 (CH$_2$*C*H$_3$)
23c	165,3, 164.8, 157.0 (2 × ester *C*O, ring *C*O), 140.4, 139.3 (2 × C=*C*), 121.0 (O*C*O), 120.3 (*C*=N), 58.9, 53,5, 53.2 (3 × O*C*H$_3$), 48.3 (*i*-Pr *C*H), 22.1 (*i*-Pr *C*H$_3$)
23d	165.5, 165.2, 157.2 (2 × ester CO, ring CO), 141.7, 138.5 (2 × C=C), 122.8 (C=N), 120.8 (OCO), 68.8 (OCH$_2$), 53.5, 53.4 (2 × OCH$_3$), 48.3 (*i*-Pr CH), 22.4 (*i*-Pr CH$_3$), 15.4 (OCH$_2$CH$_3$)
23e	165.5, 165.2, 157.2 (2 × ester *C*O, ring *C*O), 143.0, 139.5 (2 × C=*C*), 126.8 (*C*=N), 120.5 (O*C*O), 76.6 (O-*i*-Pr *C*H), 53.4, 53.3 (2 × O*C*H$_3$), 48.1 (N-*i*-Pr *C*H), 22.4, 22.1 (2 × *i*-Pr *C*H$_3$)

[a] δ values, in ppm relative to TMS, measured in CDCl$_3$ at 263 K and 75.47 MHz.

Compounds 22. The FD-mass spectra of **22** show the correct masses for the molecular ions of the free butenolides (−1H). The IR spectra of **22** show in the organic carbonyl region three absorptions around 1798, 1748, and 1720 cm^{-1}. Similar to complexes **10**, the high-frequency absorption is assigned to the lactone carbonyl. The other two bands are consequently assigned to the ester carbonyl groups. The weak absorption at ca. 1675

cm^{-1} is ascribed to the imine double bond. The ^1H NMR spectra of **22** are almost identical with those of complexes **10**. The imine proton resonances and those of the R^1 substituent on nitrogen are shifted slightly to lower frequency, and the methoxy proton resonances of the former alkyne ester groups are shifted somewhat to higher frequency. More pronounced shifts are observed in the ^{13}C NMR spectra. The alkene carbon atoms, observed at ca. 154 and 130 ppm, respectively, are shifted ca. 70 ppm to higher frequency as a result of the decoordination of the double bond, and the imine carbon resonances (154 ppm) are shifted by ca. 24 ppm to lower frequency: i.e., both normal ppm values for these types of carbon atoms. As in compounds **21**, the inserted CO and the carboxyl ester carbons (164−160 ppm) are also shifted to somewhat lower frequency upon decoordination.

Compounds 23. The FD-mass data of compounds **23** show mass peaks which are 16 *m/e* units lower than those of the corresponding free butenolides (**22**). This indicates the loss of an oxygen atom, which is supported by ^1H and ^{13}C NMR data; i.e., the same number of proton and carbon atom resonances are observed for **23** as for **22**. In the IR spectra of **23**, the high-frequency band at ca. 1797 cm^{-1}, observed for the free butenolide, has disappeared, which indicates that the five-membered butenolide ring is not present in **23**. The absorption band of the carbonyl ester groups (1744 cm^{-1}) are found at positions similar to those in **21** and **22**. The lactam carbonyl gives rise to an absorption at 1710 cm^{-1}.

Most noticeable in the ^1H NMR is the *N*-isopropyl methine proton resonance which is observed at 5.3 ppm, a shift of ca. 1.6 ppm to higher frequency compared to the normal position of this proton: e.g., in **10c**−**e**, **21c**, and **22c**,**d**. This strongly indicates a chemical change of the imine fragment. Additional information comes from the low-frequency shift (30 ppm) of the former imine carbon resonance to ca. 120 ppm and the low-frequency shift of the former imine proton to ca. 7.1 ppm, both indicating a $NC(H){=}C(R^3)$ double bond. This agrees well with the high-frequency shift (14 ppm) of the $C(R^3)$ carbon atom resonance to 120 ppm, as compared to that in **22**. The formation of this double bond is furthermore supported by the two low-frequency bands observed in the IR at ca. 1655 and 1600 cm^{-1}, which are characteristic for the present 1,3-diene fragment. The shift to higher frequency of the *i*-Pr methine protons of **23** is probably due to the proximity of these protons to an anisotropic C═O bond.

Complex Formation. To explain the formation of the observed organometallic products two separate reaction paths are proposed for the reaction with DMAD and MP, respectively (Schemes 2 and 3). It should be noted that, although the intermediates in these reactions could not be isolated or detected, their intermediacy is based on the analogy with the reactions of $Fe(CO)_3$(α-imino ketone)[8,9,56] and $M(CO)_3$(R-DAB) (M = Fe, Ru)[6,7,10] with activated alkynes (cf. Scheme 1). Therefore, before discussing the observed reactivity, it is necessary to concisely summarize some results described in earlier parts of this series. Therein we have demonstrated that the M−N═C (M = Fe, Ru) and the Fe−O═C fragments are isolobally[68,69] related to an azomethine and a carbonyl ylide, both well-known classical organic Huisgen 1,3-dipoles.[70−72] On this basis, the initial step in the reaction of $Fe(CO)_3$(α-imino ketone) and $M(CO)_3$(R-DAB) (M = Fe, Ru) with activated alkynes can be described as an oxidative 1,3-dipolar cycloaddition across the M−X═C fragment leading to the bicyclo[2.2.1] intermediate **2** (cf. Scheme 1). The initial cycloadduct **2** has been fully characterized for both the M−N═C system (M = Fe,[73] Ru[7]) and recently for the Fe−O═C[74] system as well. In analogy with the isolobally related organic ylides, it was furthermore shown that the Fe−X═C fragment (X = O, NR^1) can be classified as a nucleophilic or type I 1,3-dipole according to the Sustmann classification.[11−15,75] This is supported by the outcome of some preliminary CAS-SCF calculations performed on both the organic ylides and the model systems $Fe(CO)_3(HN{=}C(H)C(H){=}X)$ (X = NH, O),[8,76] which showed that they are electron-rich species and possess high-lying HOMO and LUMO levels. Cycloaddition reactions of these types of 1,3-dipoles are HOMO-controlled; i.e., the interaction of the dipole HOMO and the dipolarophile LUMO is predominant, and they react preferentially with electron-deficient dipolarophiles, which is in line with the observed reactivity.

Furthermore, it has been shown that in the reaction of $Fe(CO)_3$(α-imino ketone), in which both the Fe−N═C and Fe−O═C fragments are present, the activated alkyne exclusively reacts over the Fe−O═C fragment, indicating that this fragment is more reactive due to electronic and steric reasons.[8] As has been shown by Houk et al.,[17,18] substituents on both the dipole and the dipolarophile have a significant influence on the frontier orbitals (energy and coefficients), which can strongly affect the relative reaction rates or regioselectivity of the (organic) cycloadditions. Introduction of an electron-withdrawing group on a terminus of the 1,3-dipole will lower the HOMO energy level and thus, in the case of a HOMO-controlled cycloaddition, to a decrease in reactivity. This effect has been demonstrated in the α-imino ketone system for the cycloaddition across the $Fe{-}O{=}C(R^3)$ (R^3 = Me, Ph) fragment with DMAD and MP, which is more sluggish for R^3 = Ph than for R^3 = Me. In the present case, the introduction of the electron-withdrawing R^3 = O-alkyl substituent on the carbonyl carbon should therefore lead to an even larger decrease in reactivity of the Fe−O═C fragment. Consequently, this may lead to competition between cycloaddition across the Fe−O═C and Fe−N═C fragments. The ratio of cycloaddition over the Fe−O═C vs cycloaddition over the Fe−N═C fragment can also be influenced by the steric bulk of both the imine R^1 (*n*-Pr → *t*-Bu) and the R^3 (OMe → O-*i*-Pr) substituents. In the following we will

---

[68] Hoffmann, R. *Science* **1981**, *211*, 995.
[69] Hoffmann, R. *Angew. Chem.* **1982**, *94*, 725.
[70] Huisgen, R. *Angew. Chem.* **1963**, *75*, 604.
[71] Huisgen, R. *J. Org. Chem.* **1976**, *41*, 403.
[72] Huisgen, R. *1,3-Dipolar Cycloaddition Reactions*; Wiley: New York, 1984.
[73] Frühauf, H.-W.; Seils, F.; Stam, C. H. *Organometallics* **1989**, *8*, 2338.
[74] Siebenlist, R.; Frühauf, H.-W.; Vrieze, K.; Smeets, W. J. J.; Spek, A. L. To be submitted for publication.
[75] Fukui, K. *Acc. Chem. Res.* **1971**, *4*, 57.
[76] Dedieu, A.; Liddel, M. J. Unpublished results.

first discuss the reactions with DMAD and MP and, subsequently, the decomplexation reactions will be discussed.

Reaction with DMAD. For all ligands employed the main reaction is a cycloaddition over the Fe−O═C fragment, which indicates that this fragment is still more reactive than the Fe−N═C fragment. The cycloaddition over the Fe−O═C fragment results predominantly in the formation of the $Fe(CO)_3$(butenolide) complexes **10** together with a very small amount of the binuclear complexes **11**. Besides cycloaddition over the Fe−O═C fragment, also cycloaddition is observed over the Fe−N═C fragment, resulting in either complex **13** or **15** depending on the bulkiness of the R^1 substituent. In the following the formation of complexes **10**, **11**, **13**, and **15** and the influence of R^1 and R^3 on the course of the reaction are discussed.

Formation of $Fe(CO)_3$(butenolide) (10). The initial step in the proposed mechanism for the formation of complexes **10** and **11** (Scheme 2a) is described as an oxidative 1,3-dipolar cycloaddition over the Fe−O═C fragment, resulting in the [2.2.1]bicyclo intermediate **8**. At this point intermediate **8** has two options: it can either react intramolecularly with CO to complex **10** or it can react intermolecularly with an $[Fe(CO)_4]$ fragment to form complex **11** (vide infra). Intramolecularly, intermediate **8** reacts further, via the "normal" route, by insertion of a terminal CO ligand in the Fe−O bond. Subsequent uptake of an additional CO ligand results in the coordinatively saturated bicyclo[2.2.2] intermediate **9**. Analogous to the reactions of $Fe(CO)_3$(α-imino ketone), intermediate **9** could not be detected spectroscopically because it isomerizes very rapidly via reductive elimination of the two Fe−C σ-bonds, i.e., by C−C bond formation and subsequent recoordination of the double bond, to form the $Fe(CO)_3$(butenolide) complex **10**.

Formation of 11. Instead of insertion of CO in the Fe−O bond, intermediate **8** can also react with $Fe(CO)_4$ fragments present in the reaction mixture. Complexes **11** are formed in very low yield (±1%) for all ligands employed, which indicates that insertion of CO is much faster than the reaction with $Fe(CO)_4$. Complexes **11** are obviously formed by initial addition of $Fe(CO)_4$ (isolobally related to a carbene) to an iron−C bond of a terminal CO in **8** (i.e., the Fe−C bond is in its resonance structure, Fe═C═O, isolobally related to an olefin), resulting in intermediate A (cf. Scheme 6). This is how many other ligand-bridged binuclear iron complexes are formed.[35,77,78] Subsequent coordination of the C═C π-bond (intermediate B), followed by consecutive coordination of the oxygen atom with concomitant extrusion of two CO ligands, completes the structure of **11**.

Alternatively, complexes **11** could be formed by a mechanism as proposed by Muller et al.[39,40] for the isostructural $RuM(CO)_{5,6}$(AIB) (M = Fe, Ru) complexes. The formation of these complexes is described as a reaction of the alkyne carbon to the activated μ_2(N),η^2-(C═N) coordinated imine carbon atom in $MRu(CO)_6$(R-DAB). However, such a mechanism seems less likely because $Fe_2(CO)_6$(R-DAB) and $Fe_2(CO)_6$(α-imino ketone) do not form AIB or OIB types of complexes when reacted with DMAD. Furthermore, this mechanism requires a μ_2(O),η^2(C═O) coordination mode of the α-imino ester, which has never been observed.[35] In contrast, on the basis of the preceding observations it could well be that the $RuM(CO)_{5,6}$(AIB) complexes are formed via a 1,3-dipolar cycloaddition reaction. For this it is necessary that the R-DAB ligand becomes σ(N):σ(N′) coordinated to the Ru center of the binuclear complex, i.e., decoordination of the C═N double bond, which is obviously an unstable coordination mode. Subsequent cycloaddition of the alkyne over the Ru−N═C fragment, followed by a σ,π rearrangement of the former alkyne in the case of the FeRu complex, results in the formation of the $RuM(CO)_{5,6}$(AIB) (M = Fe, Ru) complexes.

Scheme 6. Proposed Reaction Mechanism for the Formation of 11

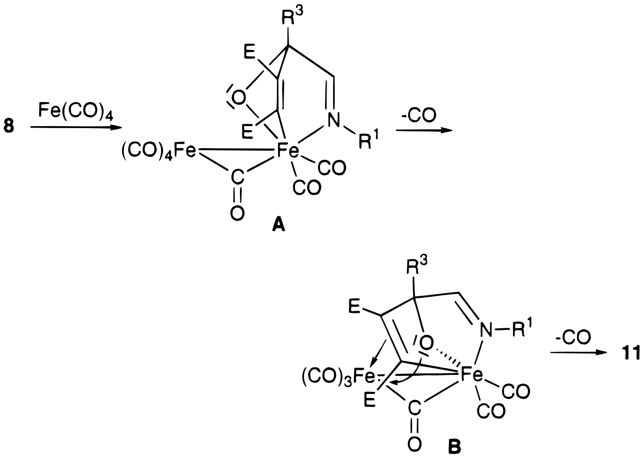

Formation of Complexes 13 and 15. The initial step in the formation of complexes **13** and **15** is an oxidative 1,3-dipolar cycloaddition over the Fe−N═C fragment, resulting in the [2.2.1]bicyclo intermediate **12**. Analogous to the cycloaddition over the Fe−O═C fragment, the reaction coordinate branches at this point. Intermediate **12** either reacts further intermolecularly with iron carbonyl to complexes **13** or reacts intramolecularly by insertion of a terminal CO toward complexes **15**. The product distribution is determined by the bulkiness of the imine nitrogen substituent R^1. In analogy to the formation of **11**, complexes **13** are formed by initial addition of $Fe(CO)_4$ to the Fe═C bond of a terminal carbonyl in **12**, resulting in the intermediate C (cf. Scheme 7). Subsequent coordination of the C═C π-bond with concomitant loss of CO results in the formation of intermediate D, analogous to intermediate B (cf. Scheme 6). A consecutive 1,2-H shift of the former imine proton to the lone pair of the amido nitrogen leads to the formation of the allylic system. Concomitant decoordination of the weakly coordinated O═C(R^3) oxygen and a change from a bridging to a terminal CO completes the structure of **13**.

Complexes **13** are only formed with the less bulky N−R^1 substituted ligands **a** (*n*-Pr) and **c** (*i*-Pr). Apparently, the incoming $Fe(CO)_4$ fragment can only approach the Fe−C bond of a terminal CO in **12** when the aminato nitrogen bears a relatively small R^1 group. Therefore, one might assume that the incoming $Fe(CO)_4$ group is precoordinated to nitrogen, i.e., bringing the $Fe(CO)_4$ in the proximity of the iron center before addition to

---

[77] Frühauf, H.-W.; Breuer, J. *J. Organomet. Chem.* **1984**, *277*, C13.

[78] Siebenlist, R.; Frühauf, H.-W.; Vrieze, K.; Smeets, W. J. J.; Spek, A. L. *Eur. J. Inorg. Chem.* **2000**, 907−919.

Scheme 7. Proposed Reaction Mechanism for the Formation of 13

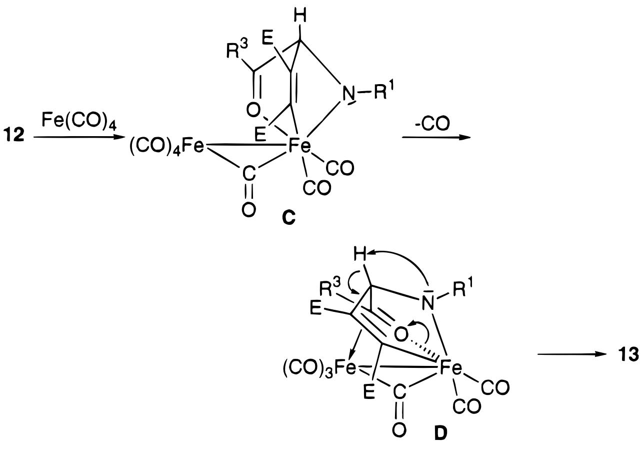

Scheme 8. Reaction of $Fe(CO)_3[\sigma(S){:}\sigma(S')\text{-}S{=}CN(CH_3)CH_2CH_2N(CH_3)C{=}S]$ with DMAD

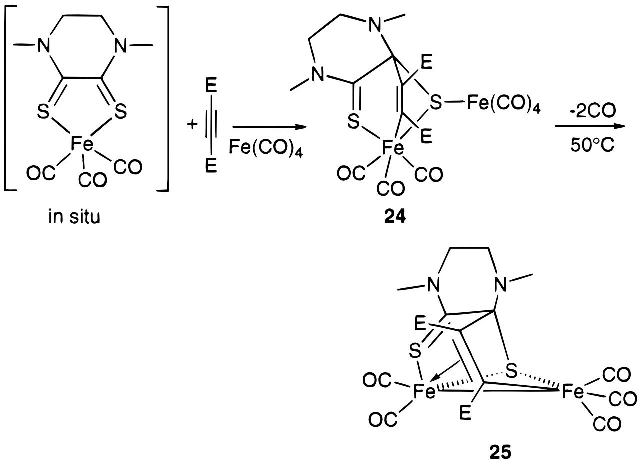

the Fe−C bond takes place. Such a precoordination of $Fe(CO)_4$, although to sulfur which is obviously a much better ligand than nitrogen, is observed as a stable intermediate (**24**) (cf. Scheme 8) in the reaction of $Fe(CO)_3[\sigma(S){:}\sigma(S')\text{-}S{=}CN(CH_3)CH_2CH_2N(CH_3)C{=}S]$ with DMAD,[79] finally resulting in complex **25** (i.e., isostructural with **11** except for the opposite σ,π coordination of the alkene).

When the addition of $Fe(CO)_4$ to the Fe−C bond in **12** is slow compared to the insertion of CO into the Fe−N bond, complexes **15** are formed via the "normal" route. Insertion of CO is followed by the uptake of an additional CO ligand, and subsequent isomerization via reductive elimination results in the formation of the $Fe(CO)_3$(pyrrolinone) intermediate **14**, analogous to complexes **4** (cf. Scheme 1; X = NR^1). Intermediate **14** subsequently undergoes a substitution of the coordinated $O{=}C(R^3)$ carboxyl oxygen by CO, due to the much weaker coordination of the carboxyl oxygen to iron in **14** compared to the imine nitrogen in **4**, to form the final $Fe(CO)_4$(pyrrolinone) product **15**.

Influence of the R^1 and R^3 Substituents on the Course of the Reaction. Both the R^1 and R^3 substituents influence the course of the reaction. First the influence of R^1 on the overall yield and subsequently the influence of R^1 and R^3 on the ratio of cycloaddition over the Fe−O=C vs Fe−N=C fragment will be discussed. In the second part the influence of R^1 on the reaction pathway of the [2.2.1]bicyclo intermediate **12**, i.e., formation of either **13** or **15**, together with the influence of R^3 on the product formation, is discussed.

Influence of R^1 on the Overall Yield. In the preceding paper[35] we demonstrated that the R^1 substituent has a large influence on the formation of the starting chelate $Fe(CO)_3$(α-imino ester) complexes (**7**). It was shown that for the bulky R^1 substituted ligands **f**−**j**, the formation of complex **7** is more efficient than for the less bulky substituted ligands **a**−**e**; i.e., higher concentrations of the chelate complexes **7f**−**j** are formed as compared to **7a**−**e**. This agrees well with the generally higher overall yields observed for cycloaddition of the bulky R^1 substituted ligands **f**−**i** while for the less bulky R^1 substituted ligands the overall yields are significantly lower and decrease with decreasing bulkiness (**c** → **a**) of the R^1 substituent.

Influence of R^1 on the Cycloaddition over the Fe−O=C vs the Fe−N=C Fragments. Within the chelate complexes **7** the R^1 substituent influences the ratio of cycloaddition across the Fe−O=C vs the Fe−N=C fragment. On basis of steric constraints, the Fe−N=C fragment will become less accessible with increasing bulkiness of the R^1 substituent, and therefore cycloaddition over the Fe−N=C fragment is disfavored. This effect is clearly shown by the reactions of ligands **a** (*n*-Pr), **c** (*i*-Pr), and **f** (*t*-Bu), all bearing the same R^3 (OMe) substituent, in which the ratio of cycloaddition across the Fe−O=C vs Fe−N=C increases from 2 (**a**) to 3 (**c**) to 21 (**f**). It must be emphasized, however, that the products formed upon cycloaddition to the Fe−N=C fragment are not the same for ligands **a**, **c**, and **f**, respectively. Therefore, it cannot be excluded that the apparent preference for reaction across the Fe−O=C fragment in ligand **f** is too high due to decomposition of **15f** during workup; i.e., complexes **15** have shown to be less stable than complexes **13a**,**c**. However, it is still clear that addition over the Fe−O=C is favored with increasing bulk of the R^1 substituent.

Influence of R^3 on Cycloaddition over the Fe−O=C vs the Fe−N=C Fragments. The R^3 substituent also influences the ratio of cycloaddition across the Fe−O=C and Fe−N=C fragments due to its steric interaction with the incoming alkyne. In earlier parts it was shown that when the cycloaddition reaction is performed with a C-substituted R-DAB ligand ($R^1N{=}C(Me)(H)C{=}NR^1$), the cycloaddition takes place exclusively on the unsubstituted carbon atom. Likewise, by increasing the bulkiness of the R^3 substituent on the $Fe{-}O{=}C(R^3)$ carbon atom (i.e., OMe → O-*i*-Pr) the cycloaddition over this fragment will become less favorable and consequently cycloaddition over the Fe−N=C fragment becomes more favorable. This steric effect is clearly demonstrated within the ligand series **c** → **e** (R^1 = *i*-Pr) and **f** → **h** (R^1 = *t*-Bu), which both show a decrease in yield for the formation of complexes **10** with increasing bulk of the R^3 substituent (cf. Table 1). As expected, the yields decrease only marginally from a OMe to a OEt substituent because the steric bulks are very similar,

---

(79) Siebenlist, R.; Frühauf, H.-W.; Vrieze, K.; Veldman, N.; Kooijman, H.; Spek, A. L.; Goubitz, K.; Fraanje, J. To be submitted for publication.

while for the more bulky O-*i*-Pr substituted ligands **e** and **h** a significant decrease in yield is observed. At the same time the yields for the formation of **15** increases (within the ligand series **f** → **h**), which shows that cycloaddition over the Fe−N=C fragment becomes more favorable with increasing bulk of the R^3 substituent. It must be noted, however, that the increase in yield for the formation of **15** (4% → 10%) does not compensate the decrease in yield for the formation of **10** (64% → 25%). This difference can probably be attributed to the collective steric effect of the O-*i*-Pr and *t*-Bu groups. In an earlier work[6] it was shown that bulky substituents on R-DAB (both on nitrogen as on the central carbon atoms) can result in a high degree of decomposition during the isomerization of the bicyclo[2.2.2] intermediate **3** to **4** (cf. Scheme 1; X = NR^1). Apparently, the combination of the bulky *t*-Bu group together with the relatively large O-*i*-Pr group leads to decomposition during the isomerization step to either complex **10** or **15**.

Influence of R^1 on the Formation of either 13 or 15 and the Influence of R^3 on the Formation of 13. When the cycloaddition has taken place over the Fe−N=C fragment, the R^1 substituent plays an decisive role in the subsequent reaction of the initially formed intermediate **12**, i.e., formation of either complex **13** or **15**. When the R^1 substituent on nitrogen is sterically less demanding, the aminato nitrogen lone pair is easily accessible for precoordination to $Fe(CO)_4$, and accordingly insertion of CO does not take place, resulting in predominant formation of complexes **13**. In contrast, for the more bulky R^1 substituted ligands **f**−**j**, precoordination is hampered or even prevented, resulting in the formation of **15**. Surprisingly, with the N-*i*-Pr substituted ligands **d** (R^3 = OEt) and **e** (R^3 = O-*i*-Pr) complexes **13d**,**e** are not formed. The R^3 substituent is not very likely to impede the reaction of **12** with $Fe(CO)_4$; therefore, there must be adverse steric interactions of R^3 with R^1 and/or the ester group (E) along the way to **13**. Similarly, no formation of **13b** (R^1 = Np, R^3 = OMe) is observed, probably due to the same reason. With ligands **b**−**e** small amounts of complexes **15** are formed (observed by NMR), which demonstrates that with these ligands, apart from reaction with iron carbonyl, insertion of CO in the Fe−N bond also takes place.

Reaction with MP: Formation of Complexes 16, 19, and 20. Reaction with the less activated alkyne MP results in regioselective cycloaddition across the Fe−O=C fragment, which once more shows that this 1,3-dipolar fragment is more reactive than the Fe−N=C fragment. The first step in the reaction is described as a 1,3-dipolar cycloaddition of MP over the Fe−O=C fragment, resulting in the formation of the bicyclo[2.2.1] intermediate **8** (cf. Scheme 3) with the unsubstituted alkyne carbon added to the iron center. The same regioisomer is formed in the reaction of $Fe(CO)_3$(α-imino ketone) with MP (cf. Scheme 1).[9] In the latter case, it was demonstrated that the formation of this regioisomer can to a large extent be rationalized by the theoretical concept for cycloaddition reactions developed by Houk et al.[17,18] Intermediate **8** reacts intramolecularly further by insertion of CO into the Fe−O bond, i.e., formation of a coordinatively unsaturated bicyclo[2.2.2] intermediate. This intermediate has two options to react further, depending on the additional ligand available. Reaction with CO, i.e., the "normal" route, results finally in the formation of complexes **16**. When instead of CO this intermediate reacts with MP, intermediate **17** is formed in which the alkyne is π-coordinated to iron. Isomerization of **17** via reductive elimination results in the formation of the butenolide intermediate **18**, which is formed prior to C−C coupling. This is supported by the observation that complexes **20** are also formed in high yields upon irradiation of the butenolide **16** in the presence of an excess of MP. Subsequent C−C coupling of the unsubstituted carbon of the coordinated MP with the unsubstituted carbon of the π-coordinated double bond of the butenolide results in the formation of the final product **20**: i.e., the same linkage isomers as observed for **6** (cf. Scheme 1). As has been shown by van Wijnkoop et al.,[9] the observed regioselectivity is in agreement with the theoretical concept for C−C coupling reactions developed by Stockis and Hoffmann.[80] The preferred linkage isomer is the one that has the largest lobes of the π^*-orbitals of both components in a β-position to the metal. Since the largest lobes reside on the unsubstituted carbon atom,[81] the observed regioselectivity is in line with the theoretical model. Complexes **19** are formed upon irradiation of complexes **10** in the presence of an excess of MP, analogous to **20**. As shown above, the observed regioselectivity is in agreement with the theory. However, it is obvious that one would expect this isomer also on steric grounds. The decrease in yield observed for the formation of **19** compared to **20** is due to the increased bulk on the carbon on which the C−C coupling takes place, i.e., substitution of a proton with a methyl ester group.

The reactions with MP are performed with the three ligands **c** (*i*-Pr), **f** (*t*-Bu), and **i** (*t*-Am), all bearing the same R^3 = OMe group. The yields with the less reactive MP are significantly lower than those with the more reactive DMAD. Obviously, a considerable amount of the in situ formed chelate complexes **7** decomposes before it can react with MP or decomposes on the way to the corresponding final products **16** and **20**. It has been observed[82] that reaction of $Ru(CO)_3$(*i*-Pr-DAB) with MP initially results in the formation of the bicyclo[2.2.1] adduct. However, upon further reaction the complex decomposes. Analogously, a similar type of decomposition might reduce the yields in the present case.

In the case of ligand **c** the exclusive formation of **20c** is observed. This is attributed to the sterically less demanding R^1 = *i*-Pr substituent on nitrogen in **c**, as compared to ligands **f** and **i**. This makes the iron in **8c** more readily accessible for coordination of the relatively large additional MP ligand, thus resulting in exclusive formation of **20c**. When the alkyne MP (2 equiv) is added in one lot, the yields for complexes **20** are, as expected, increased. However, complexes **16f**,**j** are still formed because the uptake of an additional CO is obviously competitive.

Formation of Butenolide 21. Heating a THF solution of complexes **10** to 75 °C probably results in the formation of an organometallic intermediate which, in

---

[80] Stockis, A.; Hoffmann, R. *J. Am. Chem. Soc.* **1980**, *102*, 2952 and references cited therein.
[81] Libit, L.; Hoffmann, R. *J. Am. Chem. Soc.* **1974**, *96*, 1370.
[82] van Wijnkoop, M. Personal communication.

the IR, shows no terminal ν(CO) stretching bands. Subsequent reaction of this intermediate with H_2O gives compounds **21**. In toluene, compounds **21** are formed in low yield after hydrolysis. Apparently, THF acts as a stabilizing ligand in the formed intermediate. This is supported by the presence of two broad ^{1}H NMR resonances at 1.85 and 3.5 ppm, indicative for coordinated THF, although it must be emphasized the ^{1}H NMR was broad due to the presence of paramagnetic species. Attempts to purify the intermediate by column chromatography on silica gel or filtration over Celite both failed, because this resulted in the formation of **21** and/or decomposition is observed. In the organic carbonyl region, the IR spectrum of the intermediate shows three bands of medium intensity at 1747, 1678, and 1650 cm^{-1} (CH_2Cl_2; **10f** → intermediate). These bands are shifted significantly to lower frequency compared to those of **10f** and are quite close to those of compounds **21**.

Since the composition and structure of the intermediate are not really clear, it is not possible to suggest a probable mechanism for the formation of compounds **21**. In particular it is not clear at what point and in which way the alkoxy group R^3 is lost, nor can we say if the enamine is directly formed or is a result of tautomerization of an intermediate imine.

Formation of Compounds 22 and 23. Reaction of the $Fe(CO)_3$(butenolide) complexes **10c**−**j** in toluene under 50 bar of CO pressure results in the liberation of the organic heterocycles **22c**−**j** together with $Fe(CO)_5$. Only when R^1 is a bulky substituent can the butenolides **22f**,**g**,**i**,**j** be isolated in good yield. The butenolide **22h** is isolated together with several unseparable side products. Apparently, the O-*i*-Pr group of ligand **h** has an important influence on the decomplexation reaction. Unfortunately, the isolated free butenolides are unstable and decompose on purification on silica gel and upon storage even at −30 °C. In the case of the N-*i*-Pr substituted ligands **c**−**e** two other products are formed besides the free butenolide, which confirms the influence of the R^1 substituent. One of these new products could be isolated pure and is assigned to a six-membered cyclic lactam (**23c**−**e**). The observation that compounds **23** are not formed from the corresponding free butenolides **22** indicates that the metal apparently plays a role in the formation of **23**. The mechanism, however, is not clear.

Acknowledgment. The investigation was in part supported (A.L.S.; N.V.) by The Netherlands Foundation for Chemical Research (SON) with financial aid from The Netherlands Organization for Scientific Research (NWO) and by the award of a postdoctoral fellowship under the EC Human Capital and Mobility initiative (M.T.L.).

Supporting Information Available: Listings of crystallographic data for the structure determinations of compounds **10c**, **11a**, **13c**, **15h**, **19c**, and **21c**, including final coordinates of non-hydrogen atoms, hydrogen atom positions, (an)isotropic thermal parameters, bond distances and angles, and torsion angles and, for **19c**, contact distances and hydrogen bonds. This material is available free of charge via the Internet at http://pubs.acs.org.

OM991027Y